Separation and Purification of Vanillin and *p*-Hydroxybenzaldehyde from Grass Lignins

By:

Brandon Kinn
B.Sc., University of Kansas, Lawrence, 2019

Submitted to the graduate degree program in Chemical and Petroleum Engineering and the Graduate Faculty of the University of Kansas in partial fulfillment of the requirements for the degree of Master of Science.

_____

Chair: Dr. Bala Subramaniam

_____

Dr. Tom Binder

_____

Dr. Alan Allgeier

Date Defended: 11 August 2022

The thesis committee for Brandon Kinn certifies that this is the approved version of the following thesis:

Separation and Purification of Vanillin and *p*-Hydroxybenzaldehyde from Grass Lignins

Chair: Dr. Bala Subramaniam

Date Approved: 18 August 2022

Abstract

Lignin from renewable sources such as corn residue and grasses can produce a diverse range of products from food grade cellulose to fine chemicals such as vanillin and *p*-hydroxybenzaldehyde (*p*HB). Isolating the individual components from a depolymerized lignin mixture is a difficult task. The objective of this work is to experimentally demonstrate one route to isolate and crystallize vanillin and *p*HB utilizing chromatography followed by a supercritical antisolvent (SAS) process. For method development, simulated mixtures of vanillin and *p*HB that are typical of those obtained from fast ozonolysis of lignin solution were employed. Such mixtures were loaded onto a chromatography column comprised of a 500 mL silica gel bed and eluted using acetic acid (AcOH) in toluene solvent gradient. At optimal conditions (a solvent gradient of 15 to 45% v/v % AcOH in toluene and flow rate of 15.1 ± 0.1 mL/min), 98.5 ± 2.0% of vanillin and 91.1 ± 1.3% of *p*HB were recovered in separate fractions. To demonstrate the formation of dry powders of vanillin and *p*HB using SAS process, model solutions of vanillin or *p*HB in ethyl acetate (EtOAc) solution were sprayed into a high-pressure vessel containing a supercritical fluid (SCF). The SCF selectively removes the solvent from the solution droplets, precipitating the solute which is retained in the vessel by a fine filter. At the end of spraying, the solvent is eluted from the vessel using a flowing stream of pure SCF. The crystallized solids were then recovered from the vessel and analyzed using Differential Scanning Calorimetry (DSC). Three SCFs, CO_2 (P_c = 7.382 MPa, T_c = 31.04°C), ethane (P_c = 4.872 MPa, T_c = 32.17°C), and ethylene (P_c = 5.041 MPa, T_c = 9.19°C) were tested. Predicted critical loci of the binary mixture of each of these SCFs with ethyl acetate displayed a maximum in the mixture critical temperature. By operating the chamber above this maximum, a single fluid phase in the chamber (in addition to the solid phase) is ensured. While all three SCFs were successful in

crystallizing vanillin and *p*HB, the solid yields were highest in the case of ethylene. At the higher supercritical operating temperatures required for CO_2 and ethane, the aromatic aldehydes increasingly partition into the SCF+solvent phase decreasing the solid yields. Ethylene with the lowest critical temperature among the tested SCFs, enabled operation at room temperature and milder pressures of 6.9 MPa and yielded the highest recoveries of vanillin (74.8 ± 0.9 %) and *p*HB (50.8 ± 1.4%) from the vessel. The solute that escapes from the vessel in the SCF phase is partly recovered (~20%) in the condensed solvent. DSC melting point profiles of the starting materials and precipitated solids overlap, confirming that the precipitated solids are pure. These results establish that column chromatography is a viable method to separate vanillin and *p*HB as separate solvent streams and that the SAS technique is a fast process to obtain dry crystalline powders of *p*HB and vanillin from their solutions. The results also pave the way for further process optimization and scaleup.

Acknowledgments

Foremost, I would like to thank my advisor Dr. Bala Subramaniam for his support and guidance during this project. His experience and mentorship helped shape my work and allowed me the freedom to experiment with innovative ideas. I would also like to thank my project committee and defense committee. They provided the industrial experience to push this project towards a useful outcome and the fantastic opportunity to experience working at an industrial research center. Finally, I would not have been able to do this research without the funding provided by the National Science Foundation (NSF) through its Partnership for Innovation grant #1919267 and the KU Chemical and Petroleum Engineering Fellowships which generously paid for this work. I would also like to extend my thanks to Dr. Derek Butler of ADM who was my mentor during my six-month NSF-funded internship at ADM.

I am grateful to all the students, employees, and faculty at the CEBC, many of whom helped me during my project. The students and staff researchers particularly helped me get started with my lab work and provided guidance from years of experience.

I would not have reached the end of this project without the support of my wife and family. They encouraged me through my long journey, and I would not be here without them.

Table of Contents

List of Figures

List of Tables

1 Introduction, Literature Review and Objectives

1.1 Corn Lignin as a Sustainable Source of Vanillin and *p*-Hydroxybenzaldehyde

Vanillin is a globally recognized flavor that is present in numerous household foods from ice cream to chocolate.[1] To date, nearly 85% of vanillin demand is supplied by petroleum based guaiacol, 14% by lignin, and <1% by natural vanilla bean extracts shown in Figure 1.1.[2] Vanillin demand is expected to grow at an annual rate of 5.5%[3] necessitating expansion of plant capacities. With a global trend towards sustainability and reducing petroleum-based products, the demand for alternative feedstocks and bio-based consumer products is increasing.[4,5]

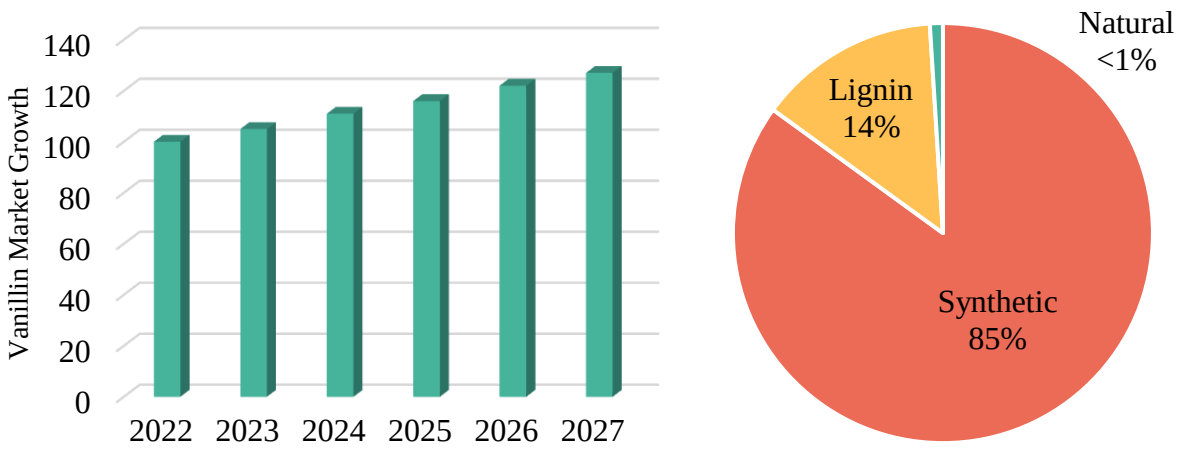

Figure 1.1: Left, projected market growth of vanillin. Right, market share of vanillin produced by synthetic, lignin, and natural sources.

Approximately 400 million tons of corn residue are produced in the US each year with a lignin content of roughly 4 million tons.[6,7] Kansas, being a top 10 corn producer at 21 million tons of corn residue per year,[8] is positioned to significantly benefit from diversifying chemicals produced by the corn industry beyond ethanol. Corn plant residue that is not utilized for making ethanol or other applications is a good source of soil nutrients and can partly offset the cost of synthetic fertilizer from lost nutrients.[9] Up to 50% of corn residue can be sustainably harvested

to be processed into lignin. The remaining corn residue represents a sustainable source of cellulose, hemicellulose, and lignin that offers other sources of revenue with increased value.

Lignin is a well-known product of hydrolyzed plant matter,[10] but not well understood.[11] It is a complex biopolymer, composed of monomeric units such as those shown in Figure 1.2, that can be processed into many different products such as specialty chemicals[12] and resins.[13–15] Kraft lignins from the paper industry[16] have been the focus of oxidation studies aimed at producing value-added chemicals. One such product is vanillin. During the past two decades, there has been increased interest in depolymerizing lignins from other sources such as bagasse and wheat to make value-added products and enhance the profitability of biorefineries that utilize these sources to make primary products such as bioethanol. In previous papers by the Subramaniam research group[17,18] it has been shown that Acetosolv processed corn residue is a viable source of lignin that can be oxidatively depolymerized (using ozone) to yield vanillin and *p*-hydroxybenzaldehyde (*p*HB) along with other low-molecular products (<1000 Da) while keeping the molecular weight distribution of the remaining lignin virtually intact for further valorization.[19,20] In addition to their use as flavoring agents, the aromatic aldehydes may also be

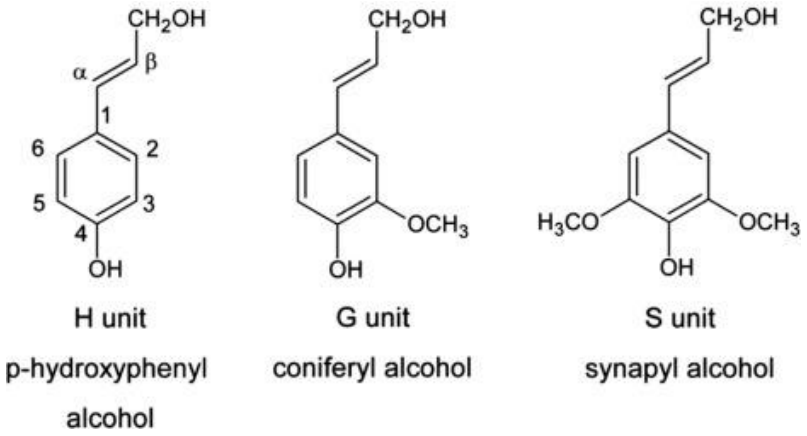

Figure 1.2: The three main repeating units of grassy lignins amorphous polymeric structure. The ratio of H:G:S units depends on the source of lignin.[19,21]

used as substitutes for petroleum-based phenol to make resins from the remaining lignin.[14]

Separating and purifying these value-added components is a difficult task and requires multiple steps involving specialized separation techniques.[21] Creating a continuous method of monomer purification is desirable for increasing throughput and reducing production cost. Vanillin and *p*HB are of particular interest as they command significantly higher prices than lignin.[22] Vanillin and *p*HB can serve as a sustainable synthetic flavorings and platform molecules for pharmaceuticals.[23,24] *p*HB can also be converted to *p*-hydroxybenzoic acid (by the Cannizzaro reaction[25,26]), where it becomes useful as a precursor for the manufacture of LCD screens.

Literature reports indicate that separating vanillin from *p*HB and other similar aldehydes prefer either a chemical modification or distillation to chromatography.[27,28] Chromatography is typically considered only for preparative scale in a laboratory but it can in some instances be scaled up. An example is the successful scaleup of column chromatography using simulated moving bed (SMB) systems to produce larger fractions of value-added components. Chromatography and SMB offer exceptional purity and good separation when tuned properly.[29] They allow the solvent (used in the separation) to be recycled and the stationary phase can be regenerated to minimize costs. Once separated, the vanillin and *p*HB must be recovered from their solutions as crystals. For accomplishing this, certain supercritical fluids (SCFs)[30] can be

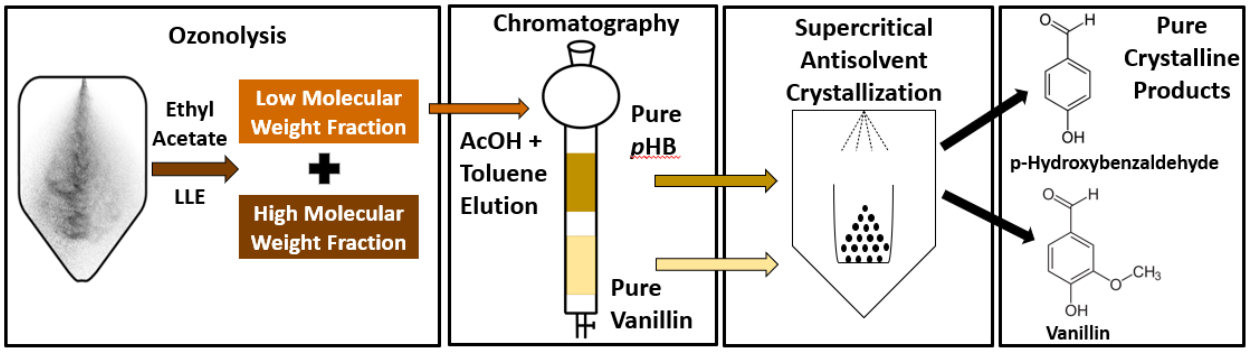

Figure 1.3: Schematic of the proposed steps to produce purified vanillin and *p*HB from grass lignins.

used as antisolvents to rapidly crystallize solutes from solution based on their tunable solubilities in SCFs.[31] This crystallization process is termed as the Supercritical Antisolvent Process or SAS.

For the separation scheme shown in Figure 1.3, the use of benign solvents and being resource efficient (i.e., conserving solvent and energy use) are essential to promote economic viability and overall sustainability. Considering these constraints, the overarching goals of this thesis are to demonstrate laboratory-scale methods for (a) separating vanillin and *p*HB as pure streams from the oxidized lignin solution using column chromatography, and (b) to crystallize vanillin and *p*HB from the separated streams in pure form using SAS process. The results from these studies are essential to perform reliable economic and environmental impact analysis of the entire process.

1.2 Literature Review

1.2.1 Lignin and Vanillin

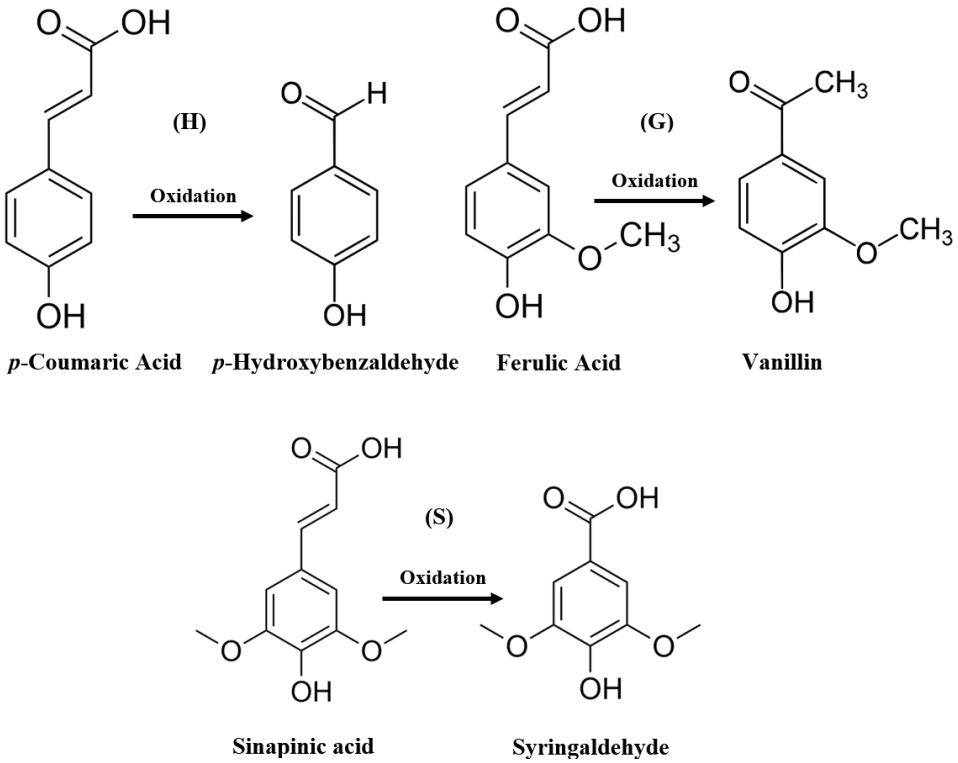

Figure 1.4: The three main building blocks of lignin and their oxidized monomers. *p*-Coumaric acid (H), Ferulic acid (G), and Sinapinic acid (S).

Lignin contains many different organic polymeric structures that make up cell walls in woody and fibrous plants.[32] The polymers are built of phenolic monomers and form a heterogenous crosslinked structure that provide strength to plants and enable them to grow against gravity.[11] The exact structure of lignins depends greatly on the plant source and method used to recover them. The most common building blocks of lignin are *p*-coumaric acid (H), ferulic acid (G), and sinapinic acid (S) units shown in Figure 1.4. These units are held together by ether (-O-) links and C=C bonds. When the lignin structure is oxidatively depolymerized in a controlled manner, the HGS units are released in various monomeric forms, such as H into *p*HB, G into vanillin, and S into syringaldehyde shown in Figure 1.4. These are just a few examples of the potential value-added products from lignin.

Vanillin (4-hydroxy-3-methoxybenzaldehyde) is a phenolic aldehyde with a 3 substituted methoxy group[33] and is the main flavonoid in vanilla flavoring. It is among the flavors directly regulated by the FDA with stringent guidelines on how consumer goods can be marketed based on the production and source of vanillin. There are three classifiers for vanillin to be sold: natural vanillin, natural flavor, and synthetic, each of which commands significantly different prices. Natural vanillin can only be extracted from cured vanilla beans and is sold at roughly $1,800 per kg.[4] Natural flavor, or just vanillin, is any method that uses natural means to synthesize vanillin, such as fermentation and non-catalytic/oxidative routes.[23] Natural vanillin sells from $50-250 per kg depending on the process and quality. Synthetic vanillin encompasses all vanillin that cannot fit into the above labels. Depending on the process, this vanillin can be sold for $9-30 per kg. To be marketable, vanillin must be >97% purity for technical applications and >99.5% for food flavoring.[34] The vanillin considered in this work falls in the synthetic vanillin category, as the use of ozone as an oxidizing agent disqualifies its labeling as natural vanillin, even though it is

sourced from a renewable naturally occurring feedstock. However, it is expected that consumers may yet prefer a sustainable rather than a petroleum source for making vanillin.

1.2.2 Industrial Methods to Produce Vanillin

Vanillin was first isolated from vanilla beans in the mid 1800's and has since boomed in popularity with a global yearly production of 26,000 metric tons in 2019[35] and a projected growth of 8%. This demand is largely met by synthetically produced vanillin. The oldest production method that is still in use is the Guaiacol synthesis route.[23] This process formylates guaiacol and its derivatives into vanillin and iso-vanillin in the presence of a superacid. Vanillin from guaiacol is considered 'synthetic' and mainly produced in China by Solvay and Merck. To separate and purify vanillin from the guaiacol reactants, a series of distillation, extraction and crystallization steps are involved. In a patent licensed to Rhodia[36] (subsidiary of Solvay), the inventors use a water wash, then a liquid-liquid extraction (LLE) under basic conditions. These steps remove some of the impurities prior to gas stripping of the residual reactants and vanillin crystallization in acidic conditions. The final vanillin purity from this process is 98.5% with 35% recovery of purified vanillin relative to vanillin present in the crude stream.

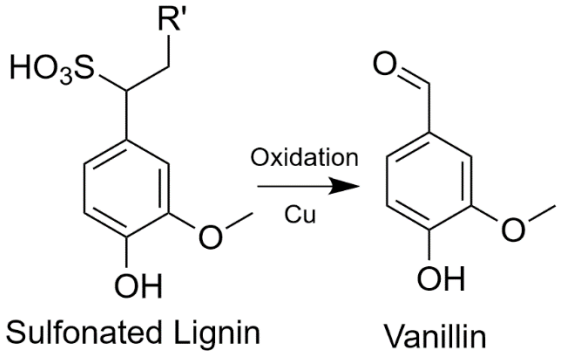

Figure 1.5: The Borregaard process (derived from the Howard process[37]) oxidizes sulfonated lignin over a copper salt catalyst. Vanillin is then reacted with sulfurous acid to form an adduct before extraction and purification

Growing desire for sustainability is the main driver to seek different methods of production. Borregaard has been producing vanillin at its Sarpsborg (Norway) facility since the 1950's.[38] They are the largest commercial producer of vanillin from lignin, specifically soft wood lignin, oxidized over a copper catalyst. To isolate vanillin from the lignosulfonate liquor,[28,39], a byproduct of the pulp and paper industry, extraction with a base is followed by treatment with sulfurous acid to form the vanillate adduct (Figure 1.5). This product is then neutralized, vacuum distilled and recrystallized. While the vanillin from this process is also considered 'synthetic', it is derived from sustainable wood instead of petroleum. As the consumer mindset shifts towards sustainably produced goods, there will be a bigger market pull to produce vanillin from other lignins and replace guaiacol-based vanillin which is currently derived from fossil sources.

1.3 Chromatographic Separation

Chromatography is an indispensable tool in analytical[40] and preparative chemistry[41]. It has a wide range of applications that utilize the three main chromatography methods, gas chromatography (GC), high-performance liquid chromatography (HPLC), and column chromatography. GC and HPLC are versatile methods for chemical analysis because of their ability to tune temperature ramp, mobile phase composition and flow rates to optimize separation, resolution, and speed.[42] Common uses include fragrance analysis,[43] alternative fuel analysis.[44] headspace sampling,[45] and natural extracts analysis.[46] Column chromatography is primarily used for preparative chemistry because it can handle larger volumes and faster flow rates to process larger quantities of the samples to be separated. All three methods use the same general principle of a mobile phase that carries the solute to be analyzed or isolated and a

stationary phase that attracts the solute and elutes it selectively. The following section discusses the basics of creating a column chromatography scheme and applications thereof.

1.3.1 Thin Layer Chromatography (TLC)

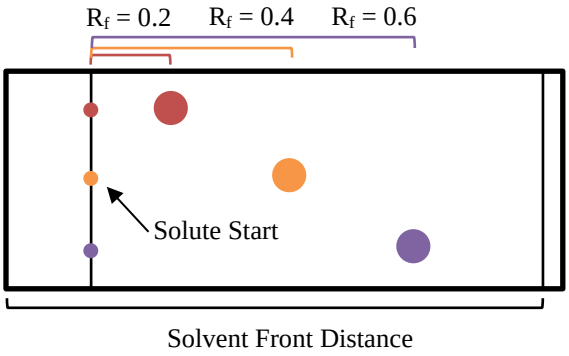

Figure 1.6: Representation of a typical TLC plate. The solutes are spotted on a line above the solvent reservoir and eluted up the plate. Their distance is measured from the line to the center of the final dot. The solvent distance is measured from the bottom of the plate to the end of its elution.

TLC is used in finding a suitable column chromatography system[47]. It allows for rapid screening of mobile and stationary phases using small paper, glass or metal plates with the stationary phase deposited.[48] TLC is performed by spotting the desired solutes to be partitioned on the TLC plate with a volatile solvent and allowing the mobile phase to elute up the plate by capillary action represented in Figure 1.6.[49] If the mobile phase has sufficient attractive force on the solute to overcome the stationary phase, the solute will travel up the plate. The difference in mobility of the solutes and mobile phase is described as the retention factor (R_f).

$$R_f = \frac{Solute\ Travel\ Distance\ (cm)}{Solvent\ Travel\ Distance\ (cm)} \qquad (Eq\ 1.1)$$

An R_f value of ~ 0.3-0.7 is desirable for the solutes in the system to perform well when scaling to a column. This screening technique is fast and gives reliable insight into column chromatography performance without the use of column packing and large volumes of solvents.

1.3.2 Column Chromatography

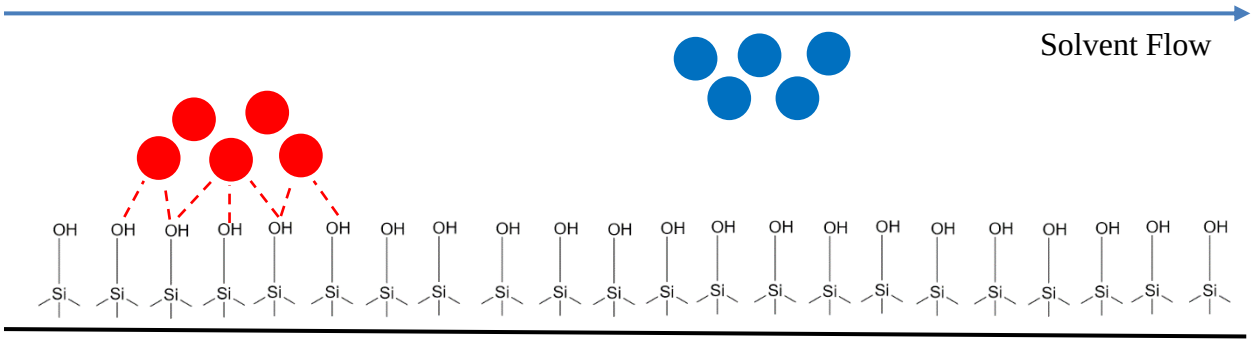

Figure 1.7: Representation of normal phase column chromatography on silica gel. The red polar solute is tightly bound to the polar silica surface while the blue nonpolar solute freely elutes with the low polarity solvent.

Scaling up from TLC to column chromatography requires knowledge of packing materials and how they affect separation. Normal and reverse phase column chromatography packings partition by polarity.[50] Normal phase chromatography involves a polar stationary phase and a non-polar mobile phase such that the first eluent is the least polar and the later eluents increase in polarity (Figure 1.7). The converse is true with reverse phase columns. Other types of packings include resins, ion exchange, and size exclusion materials.[51] The solvent system polarity determines the rate at which molecules elute from the column. By tuning the polarity, the mobility of the solute can be changed dramatically. This is important for separating two compounds, by causing them to elute either at the same time or to stay bound to the packing material for different times to effect separation. Lab scale chromatography can be done in as small as a 9” long pipette up to a 2” diameter x 16” long flash column with different types of packing materials. The most common laboratory packing material is silica gel for normal phase and C18 functionalized silica for reverse phase.

Various types of column chromatography techniques have been applied to separating vanillin from depolymerized lignin solutions. A common challenge with isolating the aromatic

aldehydes (vanillin and *p*HB) produced from lignin is the number and complexity of steps due to the similar chemistry of these monomers. Two types of chromatographic separations have been reported for fractionating oxidized kraft lignin. Gomes et al.[52,53] used a resin bed to separate using column chromatography. Vanillin from a filtered, alkaline, oxidized Kraft lignin solution was adsorbed onto the SP700 resin. It was then desorbed by water, then ethanol which removed the least, and most polar compounds, respectively. While this method isolated vanillin and *p*HB from other compounds, it did not produce pure product streams of these two compounds. Mota et al.[30] used resin-based column chromatography to perform a first separation followed by supercritical fluid chromatography (SFC) to provide a cleaner separation of the desired products. SFC will be discussed more in in a later section.

Normal phase chromatography has been utilized to isolate lignin-derived vanillin from other products by several researchers. Vigneault et al.[54] utilized flash chromatography over silica gel with ethyl ether (EE), hexane, and methanol mixture as mobile phase. The starting solution was a monomer rich fraction resulting from LLE and vacuum distillation of the product mixture from base catalyzed depolymerization of lignin that produces vanillin, catechol and syringaldehyde and derivatives of these three compounds. They concluded that flash chromatography was not suitable for the separation as many solute peaks overlapped when using EE in hexane as a solvent varying the gradient from 33%-75% followed by a methanol wash. They did however find that this system was able to fractionate dimers and trimers by desorbing with methanol. Zhao et al.[55] used a combination of Sephadex G-10 resin and silica gel chromatography to fractionate the product mixture from base catalyzed depolymerization of wheat lignin. The Sephadex G-10 packing effects separation based on size exclusion and hydrodynamic volume which can be tuned by *p*H. They found that the best recovery and purity,

78.1% and 99.6%, of monomers occurred with a mobile phase *p*H of 10.5. This initial Sephadex resin separation removed a majority of HMW compounds with m/z over 250 analyzed by HPLC-MS. To separate low molecular weight (LMW) monomers, they used silica gel chromatography with a variety of binary mobile phases using petroleum ether (PE), ethyl acetate (EtOAc), dichloromethane (DCM), ethanol (EtOH) and methanol (MeOH). They found that tuning the mobile phase polarity was important to increasing polarity by removing oligomers. PE in EtOAc was used to tune the polarity of the eluent, removing the most oligomers when using 0-50% PE in EtOAc. Above this gradient, the increased polarity helped elute the desired monomers.

1.3.3 Gradient Technique

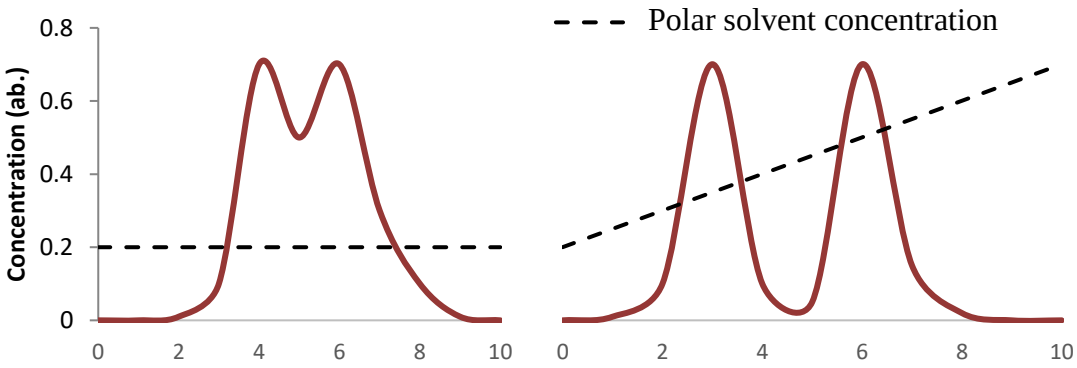

Figure 1.8: Left, isocratic chromatography, solute peaks overlap due to similar polarities. Right, applying an optimized gradient can achieve separation by increasing the polarity strength of the mobile phase.

To optimize the separation of compounds, a gradient in individual solvent flows is typically used in HPLC method development.[56] Gradient techniques in column chromatography reduce solvent use and also selectively remove solutes from the column (Figure 1.8). The basic form of column chromatography is isocratic elution where only one concentration of mobile phase (i.e., no gradient) is used. If this method is either not effective to remove solutes from the column or if the solute peaks overlap, a gradient may be used to tune the solute mobility. By tuning the polarity of the mobile phase (either increasing polarity or decreasing), the adsorbed

solutes from the column will elute faster because they will favor the mobile phase instead of sticking to the packing material, speeding up separation. This technique is used to improve separation[57] focus solute bands, and remove slow eluting solutes.

1.4 Supercritical Antisolvent (SAS) Recrystallization

Near the critical point, supercritical fluids (SCFs) display tunable density and transport properties (Figure 1.9).[58] In the near-critical region, a fluid displays unusually high compressibility. Small changes in pressure can result in relatively large changes in the fluid properties. For example, the density, heat capacity and transport properties of CO_2 (P_c = 7.38 MPa; T_c = 31.1 °C) can be varied from gas-like to liquid-like values by relatively small increases in pressure along near-critical isotherms as shown in Figure 1.9. Unique combinations of fluid properties (liquid-like densities and gas-like transport properties) can be realized at certain pressures along near critical isotherms (~ 0.9 – 1.2 T_c).

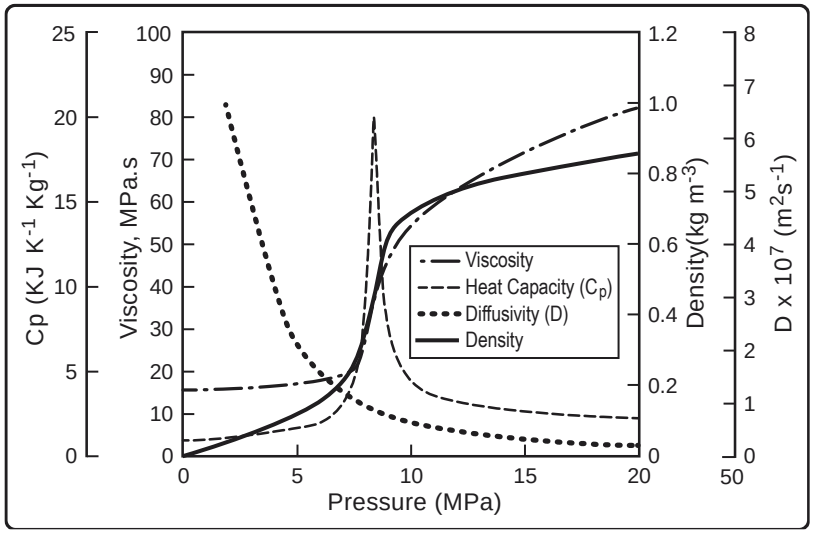

Figure 1.9: Variation of physicochemical properties of carbon dioxide near the critical point. Temperature for viscosity, density and C_p = 37 °C; Temperature for D_{11} = 50 °C.[63]

Supercritical fluids (SCF) have been known since the 1800's.[59] Within the last four decades, their applications have been constantly expanding in the areas of supercritical fluid

extraction (SFE),[60] supercritical fluid chromatography (SFC),[61] and supercritical antisolvent (SAS)[62] process. The antisolvent properties of SCFs are of particular interest because they offer low temperature, rapid, continuous, high-throughput processing options for crystallizing solutes from solution.[63–65] The gas anti-solvent process (GAS) was first introduced in 1989 by Gallagher et al.[31] They found that expanding a solvent laden with solute in a SCF caused the solute to rapidly nucleate forming crystals that varied in size based on the pressure and rate of antisolvent addition. Now, there are many different processes that utilize the tunable antisolvent properties of SCFs such as rapid expansion of supercritical solutions (RESS)[66] and precipitation with compressed antisolvent (PCA).

SAS processes are commonly used for making crystals of active pharmaceutical ingredients (APIs) that need specific particle sizes and are sensitive to mechanical and thermal stresses.[67] The SAS process offer a safe, green alternative to traditional solvent recrystallization. CO_2 is the most utilized SCF as it is abundant and is generally regarded as safe (GRAS) by the FDA for food related processing.[68] Other common GRAS SCFs include water, ethane, and ethylene with their properties summarized in Table 1.1.

Table 1.1: Critical Property Values of Common SCF[69]

Fluid	T_c (°C)	P_c (MPa)	ρ_c (g/mL)	ω
CO_2	31.04	7.382	0.4682	0.228
H_2O	373.98	22.055	0.3220	0.3449
C_2H_6	32.17	4.872	0.2067	0.1
C_2H_4	9.19	5.041	0.2142	0.086

An early method for processing depolymerized lignin by SCF was a SFE process patented by Klemola and Tuovinen[70] to extract vanillin from oxidized Kraft lignin using supercritical CO_2 (*sc*CO_2). They found that vanillin dissolved at 62°C and 22.0 MPa of CO_2

(0.735 g/mL), with considerably lower solubilities compared to other products and impurities. By tuning the density of *sc*CO_2, they were able to concentrate vanillin from 56.2% to 88.0% by selectively removing heavy oligomers from the Kraft liquor. This early work laid the foundation for lignin processing with SCFs. Since then, many researchers have investigated depolymerization in SCFs to improve yield and reduce oxygen content.[71,72] Research has also focused on the solubility of monomers in SCF for post-processing of depolymerized of lignin.[73–75]

Solubility of vanillin in SCFs is mainly a function of fluid density.[74,76,77] As a gas is pressurized beyond its critical pressure (P_c) above its critical temperature (T_c), it will become a supercritical fluid and can have densities comparable to typical solvents (Figure 1.9).[78] scCO_2, for example can vary in density from 0.4 to 0.9 g/mL[79]. Pressure-tunable density is highly desirable for a range of applications such as polymerization,[80] electrochemistry,[81] and catalysis.[82,83] Another interesting phenomenon of CO_2 and other SCFs is their ability to dissolve and expand solvents. Gases at normal and elevated pressures generally obey Henry's law of linear dissolution. When gases approach their T_c, P_c, and the solvent is easily dissolved in the gas the expansion becomes exponential resulting in over 100% expansion (ΔV) of the solvent,[84–86] as defined by Eq. (1.2) and Figure 1.10.

$$\Delta V(\%) = \frac{V(P,T) - V(P^o,T)}{V(P^o,T)} * 100 \qquad (Eq\ 1.2)$$

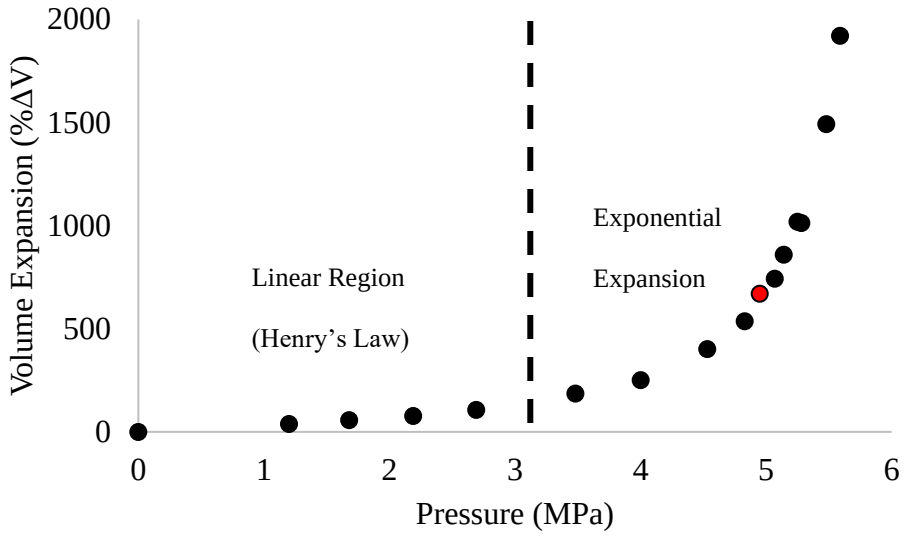

Figure 1.10 Example of solvent volume expansion in a gas above and below its critical point (•). Data of ethyl acetate in ethylene is from Kordikowski et al.[83]

The thermodynamic behavior of a binary SCF-solvent system has been classified under five different types of phase diagrams.[87,88] Even a binary SCF system can have very complex phase behavior, so it is important to fully understand the system before experiments. The most common is Type 1 phase behavior where both components are fully miscible at all compositions and the critical locus is continuous between the pure mixture critical points. Validated by experimental data, it is possible to simulate the SCF-solvent phase behavior using well known equations of state and their corresponding stability criteria.[89]

When a solid component is added to the binary SCF-organic solvent mixture, solid-liquid-vapor (SLV) equilibrium must be considered.[90,91] If the solid is soluble in the SCF+organic solvent phase, a homogenous system will form. If the solid is miscible in the organic solvent but has little or no solubility in the SCF solvent, it will precipitate from the mixture. In other words, if the solid solute was originally dissolved in a solvent, and the solvent

was then expanded using a SCF, the resulting system would involve two phases if the solid is insoluble and precipitates out of solution. This is the basis for the SAS process where rapid nucleation occurs as the solvent is selectively dissolved by the SCF causing the solute to crystallize.

Particle micronization via crystallization with *sc*CO_2 as an antisolvent allows for reproducible crystal formation with increased surface area, as demonstrated by the Subramaniam group for making insulin microparticles.[67,92] For particle micronization, ultrasonic energy is used to form droplets of drug solution. The *sc*CO_2 selectively extracts the solvent precipitating the drug. The effluent from the precipitation chamber is led to a second high-pressure vessel where the particles are separated from the solvent-laden *sc*CO_2. Collection vessel switching allows for continuous particle production. Demonstrated advantages include the continuous production of virtually solvent-free drug particles in a narrow size range and ease of process scalability to a commercial-scale crystallizer. The crystallization is a function of diffusivity of the solvent into the SCF, the nozzle type and diameter, temperature, and pressure[93–97]. A continuous SAS crystallization process is currently being practiced by CritiTech, Inc., Lawrence, KS (www.crititech.com) where kg/day of dry API powder can be produced in a continuous process.

1.5 Thesis statement

The specific objectives of this thesis are

(a) To develop a flash chromatography-based method for separating vanillin and *p*HB-containing solvent fractions from a grass lignin solution treated in a spray ozonolysis reactor to selectively produce these compounds.

(b) To obtain pure vanillin and *p*HB crystals from their solutions using the SAS process.

Outcomes from this thesis will make available new separation and purification technologies for isolating vanillin and *p*HB from grass lignin. Data from the demonstrated separation (Objective a) and purification (Objective b) processes are expected to guide the rational scaleup of these processes. They will be useful to perform technoeconomic and environmental impact analyses to guide research and development aimed at commercialization.

2 Chromatography Separation

This chapter describes the systematic investigations of various chromatographic techniques to separate vanillin and *p*HB mixed in solutions into streams containing only these components. First, TLC experiments using neat vanillin, neat *p*HB and their mixtures in various solvents are described. The results from these experiments guide the initial choice of the solid phase and solvents used in scaled-up column chromatography. Successful separation of vanillin and *p*HB mixed in ozonized lignin solution is demonstrated with high product recoveries.

2.1 Chemicals

The chemicals used in this work are summarized in Table 2.1 along with their purities (where available) and suppliers. All chemicals were used as received.

Table 2.1: Experimental Chemicals

Chemical Name	CAS	Supplier	Molecular Weight
Acetic Acid, Glacial ≥ 99.7%	64-19-7	Fisher Chemical	60.05
Acetone, HPLC ≥ 99.5%	67-64-1	Sigma Aldrich	58.08
Ethyl Acetate, HPLC ≥ 99.9%	141-78-6	Fisher Chemical	88.11
Ethyl Alcohol, ≥ 99.5%	64-17-5	Sigma Aldrich	46.07
Ethyl Ether	60-29-7	Fisher Chemical	74.12
Heptane, 99%	142-82-5	Sigma Aldrich	100.2
Hexane, HPLC ≥ 98.5%	110-54-3	Fisher Chemical	86.18
Methanol, HPLC ≥ 99.9%	67-56-1	Fisher Chemical	32.04
Petroleum Ether, ACS	8032-32-4	Fisher Chemical	
Toluene, ≥ 99.8%	108-88-3	Fisher Chemical	92.14
4-Hydroxybenzaldehyde, 98%	123-08-0	Sigma Aldrich	122.12
Silica Gel-60 (230-400 mesh) ≥ 99.5%	7631-86-9	Thermo Scientific	60.08
Vanillin, ≥ 97%	121-33-5	Fisher Chemical	152.15
Carbon Dioxide ≥ 99.5%	124-38-9	Matheson	44.01
Ethane ≥ 99%	74-84-0	Matheson	30.07
Ethylene ≥ 99.5%	74-85-1	Matheson	28.05
Nitrogen, Extra Dry ≥ 99.9%	7727-37-9	Matheson	14.01

2.2 Ozonized Lignin

2.2.1 Acetosolv Process

Corn residue is processed using the acetosolv process which is a variation of the organosolv process.[98] The specific method used for producing the lignin in this work is described in an Archer Daniels Midland (ADM) report led by Dr. Tom Binder.[99] This process has been scaled down and now utilizes corn cobs as outlined in previous work.[17] Steffan Green, an MS student in the Subramaniam group, has successfully applied this modified Acetosolv process to extract lignin from corn cobs. The acetosolv process uses 70% aq. Acetic acid (AcOH) and H_2SO_4 to hydrolyze biomass into an acid soluble fraction containing hemicellulose and lignin, and an acid insoluble fraction of cellulose. The lignin, precipitated and filtered using an excess of water, is used for further processing via ozonolysis.

2.2.2 Ozonolysis

The isolated lignin is redissolved in a AcOH/Formic Acid (FoOH)/H_2O solution before being reacted with ozone in a spray reactor demonstrated previously by Silverman et al.[17] The ozone selectively and rapidly cleaves off monomers bound to the main lignin structure via C=C bonds, resulting in partially depolymerized lignin and a liquor comprised of monomers or LMW fraction and oligomers or the high molecular weight (HMW) fraction.

2.2.3 Liquid-Liquid Extraction

The liquor obtained from the ozonolysis reactor is dried and ethyl acetate (EtOAc) is added at 50 mL/g solids. The monomers preferentially dissolve in the organic phase and can be filtered to remove most HMW compounds. The solution is filtered using a porous poly-propylene filter to remove any large solids. Then it is successively filtered using 8 μm filter paper (Whatman EW-06647-15) until the solution is clear. The filtrate or the LMW extract is the

starting material to demonstrate the chromatography-based separation process targeted in this thesis.

2.3 Chromatography Methods

2.3.1 TLC

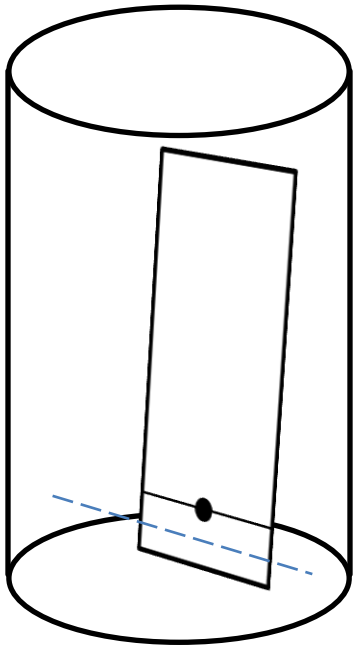

Figure 2.1: A diagram of a TLC plate developing in a sealed jar. The liquid level is marked by the dashed line and is always below the solute line on the plate.

Glass, Silica gel 60 F_{254} TLC plates, 2.5 x 7.5cm, (MilliporeSigma M1057940001) were used for screening mobile phases aimed at finding suitable solvents for chromatographic separation of vanillin and *p*HB from the ozonized lignin mixture. For screening, the plates were marked 1 cm above the solvent reservoir. One to four solute spots were marked on this line using a high volatility solvent (acetone typically) and capillary tubes. The TLC jar was filled with 5 mL of mobile phase and capped to equilibrate for 20 minutes. The TLC plate was lowered into the jar and rested at an angle such that the solvent was below the 1 cm mark on the plate (Figure 2.1). The jar was recapped, and the mobile phase was eluted up the plate until ~0.5 cm before the top of the plate and marked by a line. To visualize the solutes, a handheld UV source

(Spectroline ENF-240C) was used to fluoresce the TLC plate. The solute spots were circled, and final measurements taken to calculate the retention factor R_f. (see Eq. 1.1 for definition).

2.3.2 Column Chromatography

A 1” x 12” 250 mL fritted flash chromatography (Chemglass CG-1196-05) column was used with silica gel 60 230-400 mesh (Thermo Fisher AA42570A1) as packing. To prepare the column, 1 cm of sand was added on top of the frit to protect the silica bed. The silica gel was wetted with 1.5x bed volume (BV) of the mobile phase before being added to the column. The volume of the silica gel was measured before and after packing to determine the degree of swelling. To ensure a packing with a uniform void and no air pockets, the column was gently agitated with a rubber stopper to drive out air. To load a sample, the liquid level was lowered to just above the bed, the sample was loaded on the column wall as to not disturb the bed. After loading the sample, the liquid level was lowered to bed height and 1 cm of sand was added to protect and stabilize the bed from disturbances associated with elution before more mobile phase was added. The elution was run continuously, and fractions were collected and analyzed by either TLC or GC.

2.3.3 Flash Chromatography

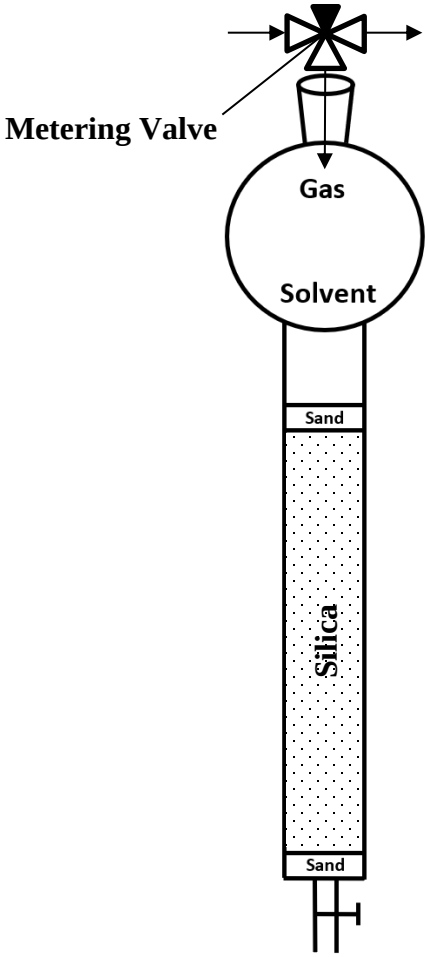

Figure 2.2: A prepared flash column with needle valve to control gas flow for safe operation. The silica bed is protected by sand caps to ensure uniform packing and to prevent from solvent disrupting the surface

Flash chromatography is prepared in the same manner as column chromatography but uses N_2 instead of gravity to drive flow. A larger 2" x 12" 1 L flash column (Chemglass CG-1197-20) is used with a chromatography metering valve (Synthware C1324) and a rotameter (Cole Palmer EW-03216-04) to control gas flow. The bed is prepared as described in Section 2.3.2 and depicted in Figure 2.2. The bed is packed using gas flow, adding needed silica to compensate for compressing the bed volume. Before loading the sample, the flow rate is adjusted as desired using a rotameter and metering valve. For safety, the gas regulator is set to 10 psig and

the rotameter is set to maintain a constant flow rate. The chromatography metering valve shown in Figure 2.2 keeps the system open to avoid pressure build up.

2.3.4 Gas Chromatography

Gas chromatography was performed using an Agilent 7890A GC equipped with an HP-INNOWax PEG column (Agilent 19091N-133) and a flame ionization detector (FID). The injector was run in split mode with a split ratio of 25:1 at a temperature of 250°C with 1 µL injections. The carrier gas (He) flow rate was 2 std cc/min. The oven temperature program was as follows: 40°C for 5 min followed by a 10°C/min ramp to 220°C where it was held for 12 min. The FID was run at 300°C. Each run had an equilibration time of 0.5 min and a post run time of 4 min. Calibrations were made using standards of vanillin and *p*HB in MeOH from 50-250 ppm to determine the GC area response. Experimental samples were prepared by dissolving the solid collected from the SAS experiments in MeOH.

A Varian CP-3800 GC equipped with an HP-INNOWax PEG column (Agilent 19091N-133), and an FID was also used to analyze chromatography fractions. The injector was run in split mode with a split ratio of 20:1 at a temperature of 250°C with 2 µL injections. The carrier gas (He) flow rate was 2 std cc/min. The oven temperature program was as follows: start at 40°C and a 25°C/min ramp to 160°C, followed by a 15°C/min ramp to 240°C where it was held for 5 minutes. The FID was run at 300°C. Each run had an oven temperature equilibration time of 0.5 minutes. Calibrations were made using standards of vanillin and *p*HB in the chromatography matrix with MeOH for diluting from 10-1000 ppm to determine the GC area response. Samples to analyze the vanillin and *p*HB fractions from the column chromatography experiments were prepared by diluting 0.1 mL of each fraction in 1 mL of MeOH. See Appendix B for calibrations.

2.4 TLC Screening

Before running column chromatography, a suitable packing material and mobile phase were determined. Model TLC was run as described in Section 2.3.1 on a variety of different mobile phases to separate vanillin and *p*HB. The results are shown in Table 2.2.

Table 2.2: Silica Gel TLC Results Using Various Solvent Systems with Commercially Sourced Vanillin and *p*-Hydroxybenzaldehyde Samples

			% Solvent		
System	*Solvent A*	*Solvent B*	*A*	$R_{f,V}$	$R_{f,pHB}$
1	Ether	Petroleum Ether	15	0.25	0.27
2	Acetone	Heptane	5, 12, 30	0.03, 0.04, 0.07	0.03, 0.03, 0.06
3	Methanol	Acetic Acid	50	0.55	0.57
4	Ethyl Acetate	Toluene	10, 10 acid, 20	0.19, 0.20, 0.31	0.15, 0.16, 0.26
5	Methanol	Acidic Water (1.25 v% AcOH)	10	Dissolved	0.81
6	Ethyl Acetate	Heptane	20, 50	0.12, 0.37	0.12, 0.37
7	Ethyl Acetate	N/A	100	0.68	0.69
8	Acetic Acid	Ethyl Acetate	3	0.65	0.67
9	Methanol	Ethyl Acetate	10	0.69	0.72
10	Ethyl Acetate	Ether	20	0.67	0.68
11	Hexane	N/A	100	0	0
12	Ethyl Acetate	Hexane	10, 50	0.04, 0.41	0.04, 0.44
13	Triethylamine	Ethyl acetate	10	0.03	Dissolved

Screening results from the separation of vanillin and *p*HB standards using TLC produced varied results depending on the solvent system (Table 2.2). These results clearly show how important the appropriate choice of solvent system is for achieving the desired separation not only for TLC but also column chromatography. Mobile phases typically consist of a polar and

non-polar solvent. The initial system (System 1) was to benchmark an educational experiment for undergrads,[100] however it produced results inconsistent with the paper. Based on the experimentally determined $\Delta R_f = |(R_{f,V} - R_{f,pHB})| = 0.02$, it would require an infeasible amount of silica to separate vanillin and *p*HB. The desired ΔR_f to scale up to column chromatography is $\Delta R_f > 0.2$ for an easy separation and $0.2 > \Delta R_f > 0.1$ for difficult separations.[47] Nearly all solvent systems in the screening set had the same R_f for vanillin and *p*HB. The set was limited to common solvent systems, with benignity being a major consideration. From this set, EtOAc and either MeOH or toluene showed minor separation with R_f's ~ 0.03 (Systems 9 and 4). While these solvents may not be suitable for standard column chromatography, they may be applicable for simulated moving bed chromatography (SMB) that offers more efficient use of the stationary phase.

The only solvent system that showed adequate separation of vanillin and *p*HB to scale up to column chromatography was AcOH and toluene. Over the tested range, the R_fs for the vanillin and *p*HB standards show a linear increase with increasing AcOH concentration (Figure 2.3). This is an ideal system for flash chromatography. Under gradient mode, the elution profile can be tuned by changing the ratio of polar (AcOH) to non-polar (toluene) solvent. Based on a ΔR_f value of 0.21 (which is just greater than the easy separation cut off), the ideal AcOH concentration in toluene to separate vanillin and *p*HB was found to be approximately 15% v/v AcOH. As the AcOH concentration is increased, the ΔR_f value approaches 0 resulting in progressively poorer separation. $R_{f,van}$ and $R_{f,pHB}$ values increase with polarity, reducing the bed volume equivalent, which is the volume of solvent required to fully elute the solute, ($BV_{equiv} \approx 1/R_f$) of solvent needed for the separation.[101]

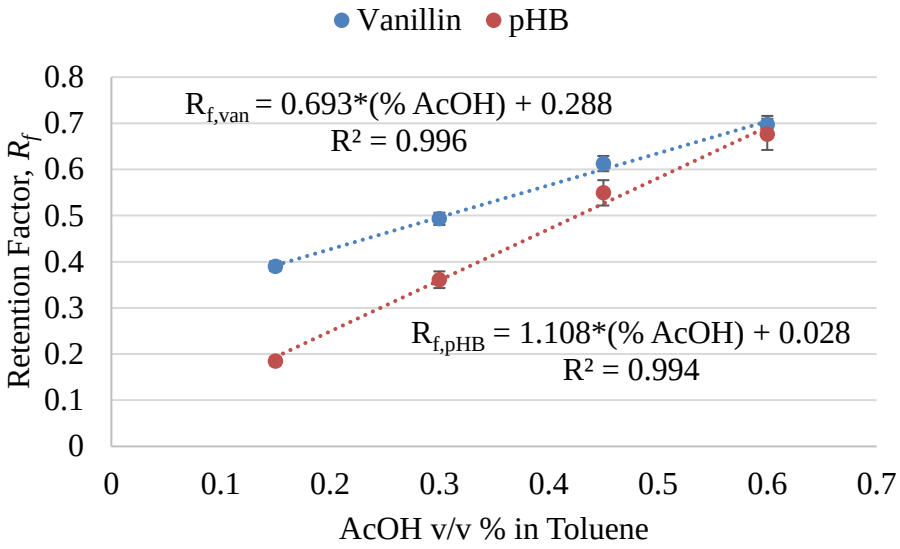

Figure 2.3: Vanillin and *p*HB both show increasing R_f with increasing AcOH fraction in toluene. Low AcOH concentrations give good separations while higher AcOH fractions provide faster elution.

Armed with a tunable solvent system for separating vanillin and *p*HB, the system was tested on the real lignin solution. The starting material was the LMW extract in EtOAc prepared as described in Section 2.2.3. The LMW was spotted on a TLC plate along with vanillin and *p*HB standard for comparison (Figure 2.4). TLC was performed using 15% v/v AcOH in toluene. From this qualitative comparison, lignin derived vanillin and *p*HB are clearly visible on the TLC plate lining up with the standards. Contaminants can be seen at the spotting line which indicates some parts of the solution are not compatible with either the solvent system or stationary phase. Based on these results, silica gel and AcOH in toluene were chosen as the system to scale up.

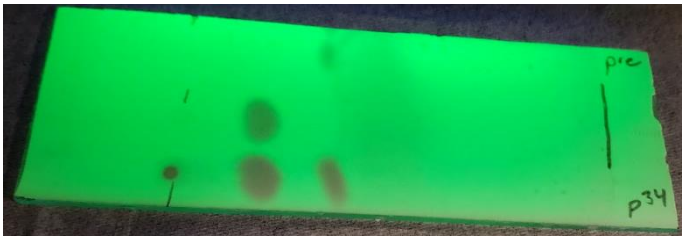

Figure 2.4: TLC plate showing elution using 15 v/v % AcOH in toluene. Top spot, vanillin standard; middle dot, *p*HB standard; bottom dot, lignin LMW extract.

2.5 Column Chromatography

The TLC results paved the way for performing column chromatography on model and real mixtures of vanillin and *p*HB using a 1” x 12” column. Initial separations were done using mixtures of vanillin and *p*HB standards, sourced commercially. Using an isocratic elution with the column properties show in Table 2.3, column chromatography was performed and analyzed qualitatively with TLC. Vanillin eluted in fractions 30-45 and *p*HB eluted in fractions 51-66. *p*HB was not fully eluted and remained in the column even after three BVs of solvent were used. This is consistent with the BV_{equiv} estimates from the TLC results. With 15% AcOH solution in toluene, vanillin and *p*HB would require 2.56 and 5.41 BVs of solvent, respectively, to fully elute.

Table 2.3: Column Chromatography Conditions for Model Mixtures

Parameter	Value
Bed Volume (mL)	80
Silica Gel 60 (g)	39.80 ± 0.02
Vanillin (g)	0.301 ± 0.02
*p*HB (g)	0.500 ± 0.02
15% AcOH in Toluene (mL)	300
Fraction Volume (mL)	5
Fractions	66

2.6 Flash Chromatography

The column chromatography results suggest that a flash chromatography procedure with a gradient technique would be necessary to completely remove *p*HB from the column. A step gradient from 15% to 45% AcOH was chosen to achieve the separation while also fully eluting *p*HB. At 45% AcOH, *p*HB has a BV_{equiv} of 1.82 which is even lower than vanillin at 15%. By eluting with 15% AcOH until vanillin comes off the column and then switching to 45% AcOH, *p*HB separation should be achieved along with its full recovery. To test this, a 2”x 12” column was used to work with larger amounts of vanillin and *p*HB. The initial loadings of 0.4 g vanillin and 1.2 g *p*HB were chosen to mimic the expected quantity of products resulting from ozonolysis of a 2 wt% lignin solution (Section 2.2.2). Other experimental parameters are shown in Table 2.4.

Table 2.4: Flash Chromatography Using Step Solvent Gradient

Parameter	Value
Bed Volume (mL)	500
Silica Gel 60 (g)	250.13 ± 0.01
Vanillin (g)	0.401 ± 0.004
*p*HB (g)	1.200 ± 0.003
15% AcOH (L) used for vanillin elution	1
45% AcOH (L) used for *p*HB elution	0.75
Flow Rate (mL/min)	15.1 ± 0.1
Fraction Volume (mL)	20
Fractions	85

The step solvent gradient technique significantly increased the speed of flash chromatography, the solute loading capacity and *p*HB recovery. The demonstrated technique displayed excellent separation (Figure 2.5). The vanillin solute peaks eluted in 30 fractions showing no overlap with *p*HB concentration. Following complete vanillin elution, the *p*HB was separated in 14 fractions. Vanillin recovery was 98.5 ± 2.0% and the *p*HB recovery was 91.1 ± 1.3%. See Appendix C for sample chromatography data.

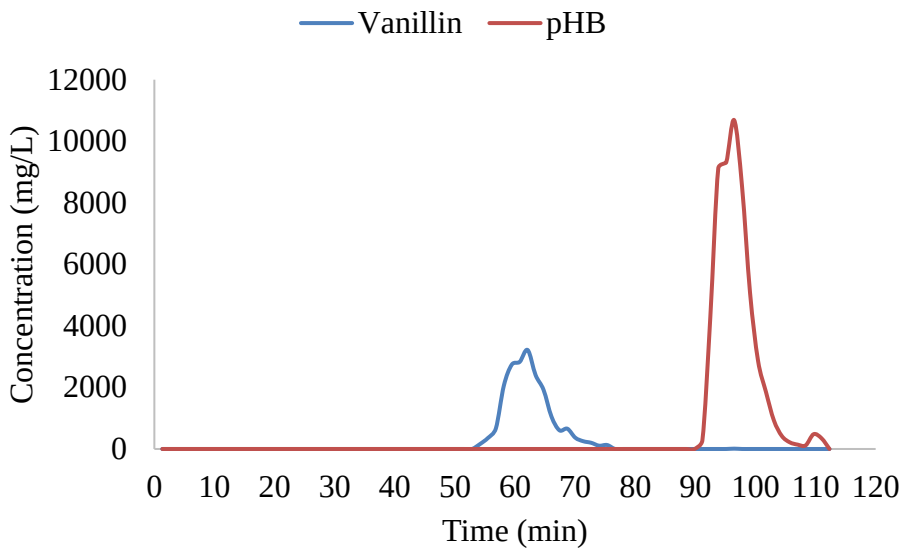

Figure 2.5: Chromatography profile of vanillin and *p*HB concentrations using the optimized 15% - 45% AcOH in toluene step gradient on silica gel.

To further check the *p*HB and vanillin mass balances, the column was washed post chromatography separation with 400 mL of MeOH. The highly polar MeOH solvent should remove *p*HB and vanillin from the silica. In the MeOH wash, 0.85 mg of *p*HB and 0.04 mg of vanillin were recovered which constitutes less than 0.1% recovery. The discrepancy is likely due to the LOD of the GC used. Vanillin is not detected lower than 10 mg/L and *p*HB is not detected below 5 mg/L. The total mass balance of the solutes (vanillin and pHB) was 92.9 ± 1.9% and the overall mass balance recovery including solvent was 97.2 ± 0.9%. The lack of mass balance

closure for *p*HB could be due to a lack of detection sensitivity in some of the samples where it exists at low concentrations. Further optimization could help to completely elute the *p*HB and improve its detection using GC-FID to close the mass balance deficit within experimental uncertainty.

2.7 Flash Chromatography of Ozonized Lignin

5.76 g of LMW extract prepared from ozonized lignin mixture was adsorbed onto 12.9 g of silica gel and loaded on top of a 300 mL silica bed. The flash column was eluted with 1.2 L of 15% AcOH in toluene which represents 4 bed volumes of solvent. 20 mL fractions were collected and analyzed qualitatively with TLC for vanillin and *p*HB separation. The results are

Figure 2.6: TLC analysis of real lignin chromatography using 15% AcOH in toluene. The top dots are vanillin recovered in each fraction and the lower dots are *p*HB in each fraction. The overlapping fractions show an incomplete separation.

shown in Figure 2.6. Vanillin eluted in fractions 25-44 and *p*HB in fractions 38-47. The unoptimized isocratic elution was not able to separate vanillin and *p*HB from a real lignin LMW fraction. However, with optimization using the step gradient, full separation is expected.

In summary, results from flash chromatography of model vanillin+*p*HB mixtures demonstrate that vanillin and *p*HB can be quantitatively separated into separate fractions using

silical gel as the stationary phase and acetic acid/toluene mixture as the mobile phase. TLC analysis of a real lignin mixture using these phases confirmed that *p*HB and vanillin in such mixtures can be qualitatively separated. These demonstrations pave the way for further scaleup and optimization using simulated moving bed chromatography.

3 Supercritical Antisolvent Crystallization

This chapter describes systematic experiments aimed at establishing the feasibility of using the supercritical antisolvent (SAS) process to crystallize vanillin and *p*HB from their solutions as pure dry powders. To demonstrate the concept, this thesis examines model organic solutions of vanillin and *p*HB as surrogates for the real solutions of these solutes isolated from ozonized lignin mixtures by column chromatography (Chapter 3). It is shown that to maximize the yields of the crystallized powders, proper knowledge of the phase equilibrium thermodynamics is essential to rationally select the SCF antisolvent and operating conditions (pressure and temperature). These aspects are described in the following sections.

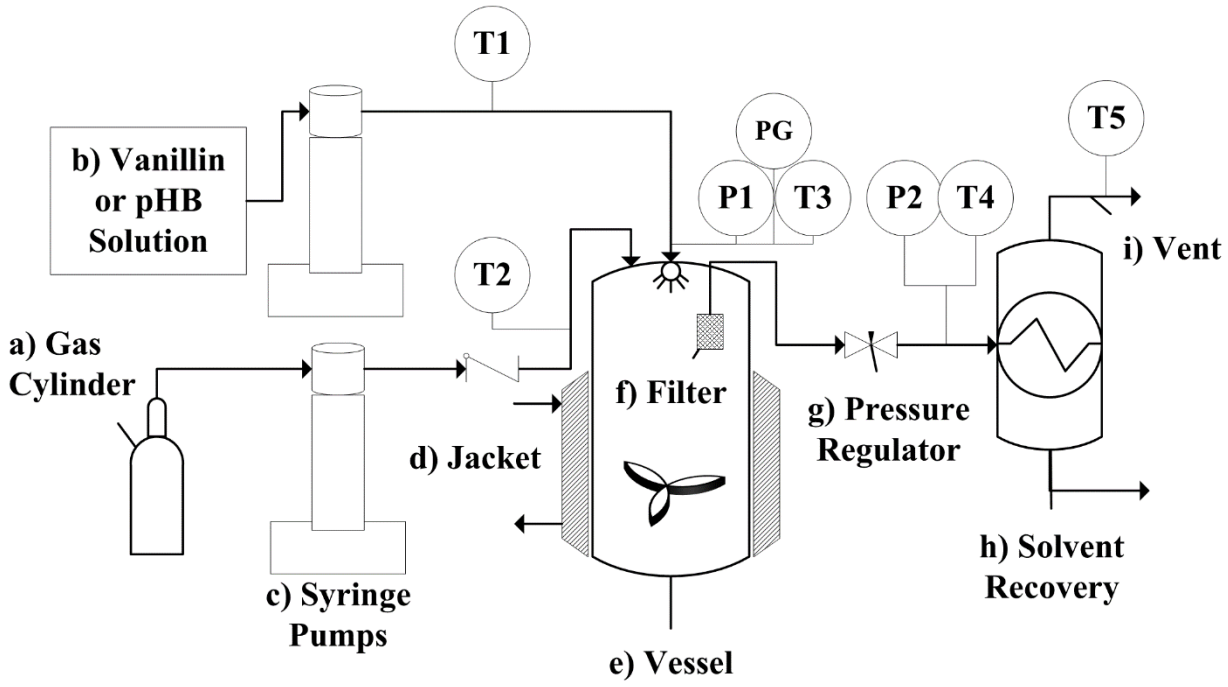

Figure 3.1: Schematic of the supercritical antisolvent (SAS) precipitation apparatus. The precipitation chamber (e) can be either a 300 mL vessel or a 50 mL vessel with appropriate heating/cooling provisions. The pressure regulator (g) was a metering valve. The thermocouple (T#) and pressure data (P#) are interfaced with a data acquisition system for real time monitoring of these variables.

3.1 SAS Methods

3.1.1 50 mL Parr Vessel as Crystallizer

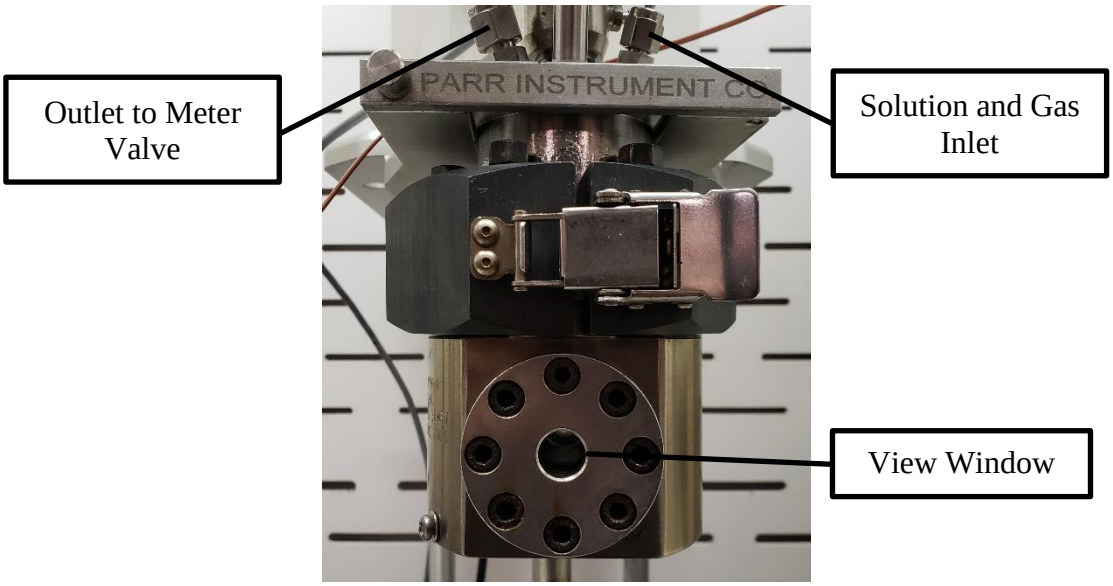

Figure 3.2: The 50 mL windowed Parr vessel used for supercritical antisolvent (SAS) crystallization experiments. The sapphire glass window allows visual observation of phases and solids formed inside the vessel.

A 50 mL Parr vessel (Parr Instruments) with sapphire view ports (Figure 3.2) was used initially in the SCF experiments to verify the occurrence of crystallization during the SAS process. The equipment consists of three main sections: the pumping section, the crystallization vessel, and the solvent recovery section. The pumping section uses two ISCO 500D (Teledyne Systems) syringe pumps, one to pressurize the antisolvent and the other to deliver the solution containing the solute at the chosen vessel operating pressure. Both pumps have heat tapes and thermocouples to monitor the temperature. The solution was delivered via a 250 μm capillary nozzle (Vici Valco T30C10D). The vessel consisted of a thermocouple, a pressure transducer, a pressure gauge, a magnetically driven stirrer, two cartridge heaters, and a filtered dip tube to retain crystallized product. Vessel pressure was maintained with a back-pressure regulator (BPR) and an inline filter was used to collect the crystallized solute. During experiments, the vessel was

wrapped with insulating tape and the BPR was heated with a heating tape wrapped with an insulation. Vessel temperature, pressure, and stir speed were controlled using a Parr 4848 controller (ParrCon) that was interfaced with a computer for recording purposes. The monitoring and recording of all other pressure and temperature instruments was done using LabView Data Acquisition System. The solvent recovery section used a 125 mL 316 SS cylinder with a dip tube to collect the organic solvent that disengages from the effluent stream of the crystallizer upon depressurization. The SCF antisolvent is released as a gas from the separator.

3.1.2 300 mL Parr Vessel as Crystallizer

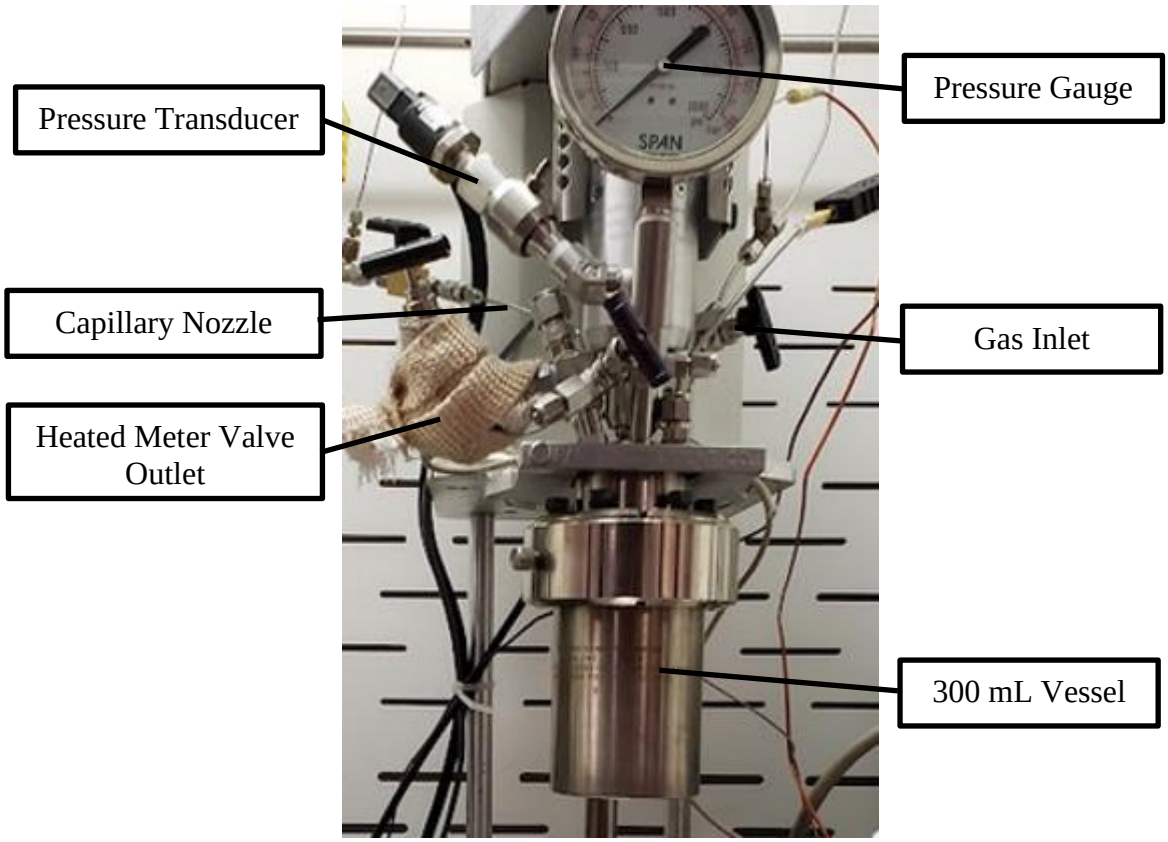

Figure 3.3: 300 mL Parr crystallization vessel. MAWP 3000 psi at 300°C, equipped with a thermocouple, a pressure gauge and transducer.

A 300 mL Parr vessel (Figure 3.3) was used in later experiments to determine optimum crystallization conditions. The 300 mL vessel replaced the 50 mL reactor in the equipment

described in Section 3.1.1 with a few key changes. A dip tube equipped with a 0.5 µm frit (Parr Inst. A3675HC) at the end to trap the precipitated solute particles and was used in place of the inline filter. An aluminum cooling jacket was used to maintain the desired crystallizer temperature. A needle valve (Swagelok SS-3NTRS4) was used in place of a traditional BPR to control and maintain the crystallizer pressure during the organic solvent wash phase. A 1L solvent recovery cylinder (Swagelok) was added along with a pressure transducer and thermocouple at the gas outlet.

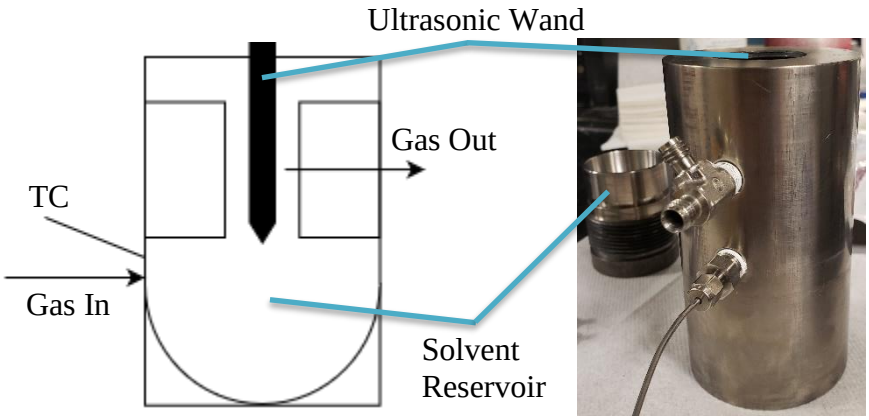

Figure 3.4: A flow diagram and picture of the VibraCell showing the gas inlet, thermocouple, and gas outlet. The gas outlet goes to a heated meter valve, used in Figure 3.3. The ultrasonic wand is suspended in the vessel to provide agitation. The solvent reservoir screws into the bottom of the cylinder.

3.1.3 VibraCell

The VibraCell (Figure 3.4) was a custom 25 mL vessel with an adapter for an ultrasonic wand (Sonics & Materials, VC 505). Gas was pumped using a ISCO 260D and pressure was monitored with a transducer while being controlled with a needle valve. The cell was at room temperature and the metering valve was heated with tape. The operating temperature was monitored with a thermocouple. The ultrasonic wand was run through the entire process, during pressurization and wash, at 40% power with a 10 second on 20 second off pulse.

3.1.4 Experimental Procedure

A typical crystallization run was comprised of four steps. The first step was to pressurize and heat the vessel with the antisolvent gas to the desired operating temperature and pressure. These are chosen such that the binary mixture of the organic solvent and SCF (antisolvent) exists in a single homogeneous phase at the operating pressure and temperature in the range of composition encountered during the spraying period. The operating pressure and temperature were predicted using phase equilibrium calculations (described later in section 3.5). The single-phase behavior was also experimentally verified using the 50 mL Parr vessel equipped with a view window. The vessel was allowed to equilibrate for 10 minutes at 1000 rpm. A fixed volume of the solution containing 100-200 mg/mL of the desired solute to be recrystallized is then sprayed into the vessel through the nozzle, such that the operating pressure and temperature are virtually unchanged. The system is allowed to equilibrate for 10 minutes to ensure that all the organic solvent has entered the SCF mixture phase, and the precipitation of the solute is completed. To recover the precipitated solute by depressurization of the vessel, the organic solvent in the SCF phase must be first removed to avoid redissolution of the solute by condensed solvent. Hence a wash is performed by flowing pure SCF at the operating T and P while keeping the system stirred and allowing the mixed phase to flow out through the pressure regulator. The SCF is flowed for 30-60 minutes, corresponding to at least six residence times in the stirred system depending on the flow rate, to remove almost all the organic solvent and leave behind a dry solid in the vessel. Once the wash is completed, the vessel is slowly depressurized over 10 minutes and cooled to room T and P. The solid is then collected from the vessel and the solvent is recovered from the downstream solvent recovery cylinder. Variations of this procedure include pre-loading the vessel with the solution of the solvent and solute (instead of spraying the

solution) and then sonicating the vessel for 30 minutes to effect through mixing of the solution and antisolvent to effect crystallization. See Appendix C for example SAS run data.

3.1.5 Differential Scanning Calorimetry (DSC)

DSC was done using a TA Instruments Q200 for melting point analysis. The DSC method used 40 std cc/min of flowing Ar to purge the cell. The temperature was allowed to equilibrate at 40°C for 2 min before ramping to 180°C at either 10°C/min or 5°C/min. Samples were prepared using a Tzero low mass pan and 5-15 mg of solid sample were added, then pressed to seal the pan. Standards of vanillin and *p*HB were used to compare the melting point profiles with the precipitated solids.

3.2 Vanillin and *p*HB Precipitation using SCFs

Precipitation of vanillin and *p*HB from SCF was initially verified using a windowed Parr vessel. The formation of solid crystals in a SCF-solvent mixture was tested by loading 6 mL of a 10 wt% solution of vanillin in ethyl acetate (EtOAc) into the vessel and pressurizing the heated reactor containing the vanillin/EtOAc solution to above CO_2+EtOAc critical point of 8.16 MPa at 40°C. After sufficient mixing, the solvent entered the SC phase. During its transition from subcritical to supercritical conditions, the phase separation becomes less apparent until the

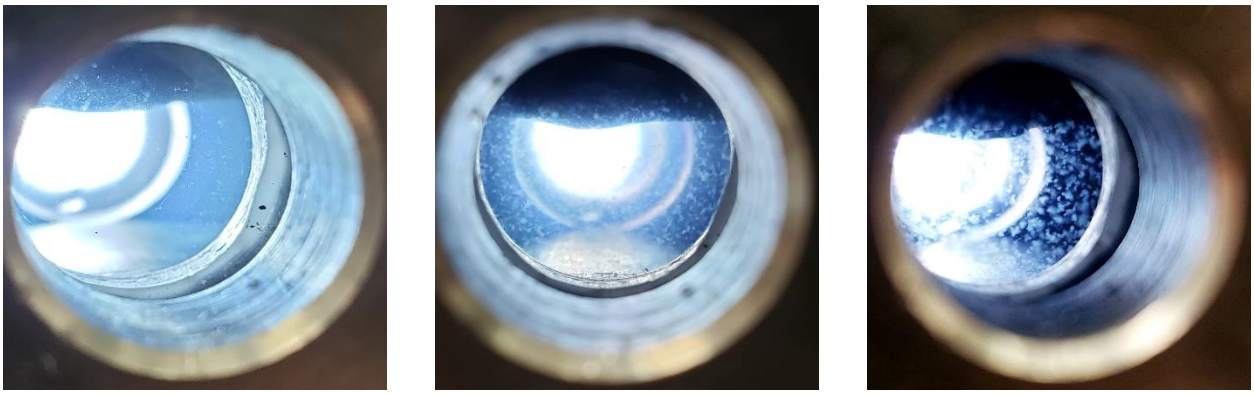

Initial Crystals | After 5 Minutes | After 15 Minutes

Figure 3.5: Crystallization of vanillin from an EtOAc solution in *sc*CO_2. The crystals can be seen floating in the clear SCF.

solution is clear as the SCF-solvent mixture becomes supercritical. In this clear phase, small vanillin crystals were visible that grew larger as they were allowed to aggregate shown in Figure 3.5. A similar experiment was performed to verify *p*HB recrystallization using *sc*CO_2 as antisolvent.

The windowed Parr vessel was then equipped with a 250 μm capillary nozzle to spray the solute containing solution and confirm that the vanillin would again precipitate from a sprayed mist. This change in solvent delivery method caused two different phenomena not observed with the process in which the solution was already loaded in the cell. Instead of floating in the solution as observed in the case with initially loaded solution, the solute particles stuck to the sides of the vessel during the spray process, coating it in a fine powder of vanillin or *p*HB. Particles that stuck to the windows were not easily recoverable. The solute also precipitated directly on the nozzle most likely due to a low flow rate of 0.25 mL/min. The addition of a nozzle greatly increased the speed of crystallization and would be useful in a continuous process.

Table 3.1: Experimental Parameters for Initial Crystallization with *sc*CO_2

Parameter	*Value*
Vessel Volume	50 mL
Temperature	40.0 ± 2.2°C
Pressure	8.27 ± 0.21 MPa
Spray Rate	0.25 ± 0.05 mL/min
Solution Volume	6.0 ± 0.1 mL
Solute Concentration	100.0 ± 0.5 mg/mL
Impeller	1000 ± 20 RPM

The windowed vessel was not suitable for recovery of the crystals due to its low volume and inability to retain particles without external filters that required heating. However, initial experiments in this vessel conclusively showed that vanillin and *p*HB can be individually

precipitated from their organic solutions using a SCF antisolvent. To facilitate easier recovery of the solute, a larger vessel equipped with a filter that can retain the precipitated particles in the vessel itself was used.

3.3 Optimizing Precipitation of Solutes with Three SCF

To determine the optimum SCF, the experimental apparatus was changed to a 300 mL Parr vessel equipped with a filter frit in a dip tube. The 0.5 μm frit was able to retain the precipitated crystals for collection and analysis. In these studies, solute recovery is defined as mass of solids (g) recovered from the vessel relative to the mass of solute sprayed (g). The molar composition of the binary organic solvent+SCF mixture is calculated using empirical density correlations[102–104] of the SCF at the operating temperature and pressure.

3.3.1 Vanillin Precipitation with Supercritical Carbon Dioxide as Antisolvent

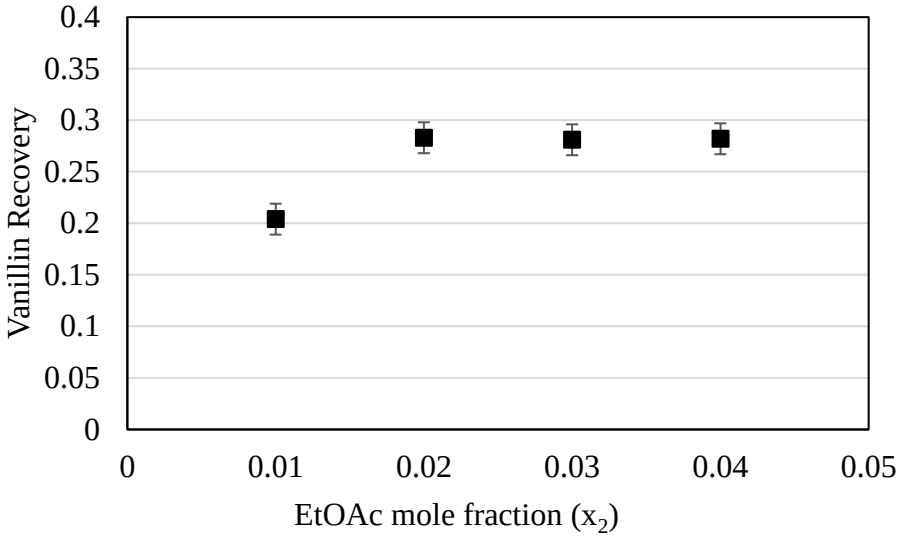

Figure 3.6: Recoveries of vanillin from *sc*CO_2 (x_1) at 40°C, 8.27 MPa and various organic solvent mole fractions (x_2).

Initial experimental pressures were chosen to be sufficiently above the maximum mixture critical point of CO_2+EtOAc system such that any change in composition would not cause the binary mixture to become subcritical. The mixture critical pressure of CO_2+EtOAc at x_{EtOAc} =

0.02 and T = 40°C was 8.21 MPa, observed in the windowed vessel, which is slightly higher than literature values of 8.16 MPa at x_{EtOAc} = 0.036 and T = 40°C.[102,105,106] Supercritical CO_2 as the antisolvent had the least recovery of precipitated vanillin at 28.3 ± 0.2% at x_{EtOAc} = 0.02 and showed no improvement with variation in the mole fraction of EtOAc (Figure 3.6).

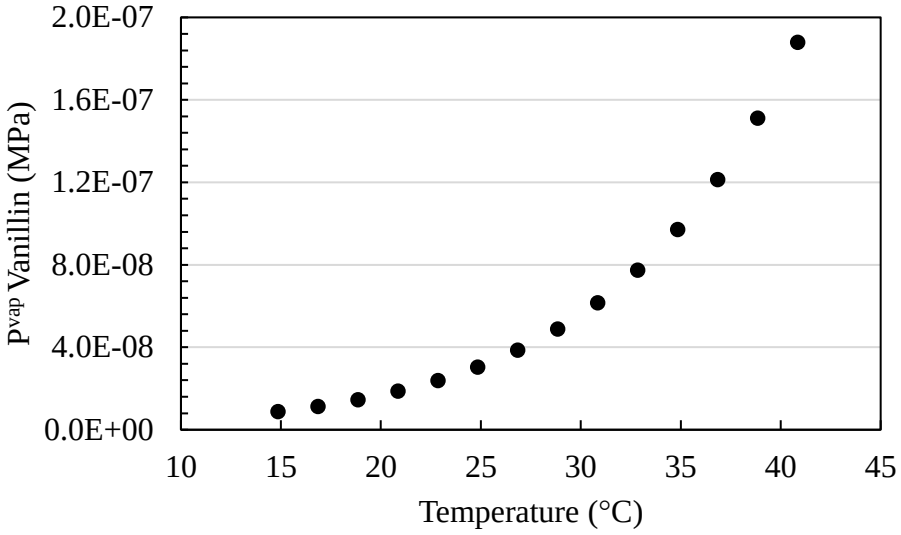

Figure 3.7: Pure component vapor pressure of vanillin over the range of experimental temperatures. Experimental data from literature[33].

Of the SCFs tested, CO_2 required the highest minimum temperatures at 31.0° C. Even though vanillin and *p*HB are solids, they exhibit measurable volatility at room temperature. Because of this, both compounds have an easily identified odor making them difficult to process without loss due to volatilization. Vanillin's pure vapor pressure as a function of temperature is shown in Figure 3.9. Increasing temperature significantly increases their vapor pressures. Between 15 and 40°C, which includes the regions just above the critical temperature of CO_2, ethane, and ethylene, the vapor pressure of vanillin increases by an order of magnitude (Figure 3.7). Consequently, SAS experiments with CO_2 and ethane resulted in lower vanillin recoveries in the vessel with a significant amount of vanillin likely escaping in the SCF+solvent phase due to volatilization of vanillin.

3.3.2 Vanillin Precipitation with Supercritical Ethane as Antisolvent

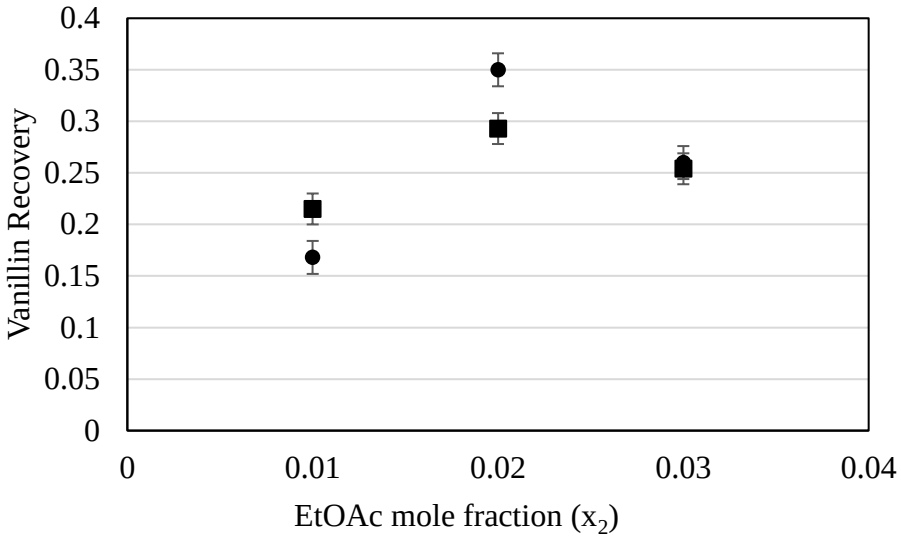

Figure 3.8: Recoveries of vanillin from *sc*C_2H_6 (x_1) at 35°C and various organic solvent mole fractions (x_2). Experimental pressures of 8.27 MPa (■), 5.51 MPa (●).

Ethane was chosen as the next SCF because it had a similar T_c (32.2°C) as CO_2 but a lower P_c (4.872 MPa) and is also a food grade solvent. The operating conditions were chosen based on reported binary C_2H_6+EtOAc mixture critical data.[103] The operating conditions to maintain a supercritical phase of the C_2H_6+EtOAc binary system are as follows: (T = 35.0°C, P = 5.514 MPa, x_{EtOAc} = 0.02).The yields of precipitated vanillin obtained with supercritical ethane were higher than with *sc*CO_2 with the best value being 35.0 ± 0.2%. The yield of vanillin from supercritical ethane as antisolvent is still low due to the vapor pressure being significant even at moderate temperatures.

3.3.3 Solubility of Solutes in SCF

SCF density is known to have significant impact on the recovery of solids. Vanillin and *p*HB are known to be soluble in *sc*CO_2[73,76] and are likely also soluble in supercritical ethane and supercritical ethylene.[107] The presence of co-solvents can also significantly increase the dissolution power of SCF by modifying its dielectric constant.[108] For example, EtOAc would

increase the polarity of the SCF phase leading to stronger dissolution of polar compounds. Vanillin and *p*HB are both polar compounds, with *p*HB being more polar, both readily dissolve in polar solvents such as chloroform, EtOH, MeOH, and EtOAc. Ethylene, by virtue of its lower critical temperature and pressure, allows operation at much lower densities of the SCF phase compared to operation with *sc*CO_2 and supercritical ethane. The combination of lower vapor pressure and lower SCF densities, allowed by operation with supercritical ethylene, results in higher vanillin recovery. Hence, ethylene was chosen as the optimum SCF for further experiments.

3.3.4 Modeling of Vapor Liquid Phase Behavior of Ethylene-EtOAc System

With ethylene-EtOAc selected as the desirable solvent for the SAS system, preliminary modelling was done to predict the critical loci of the binary system and thereby to guide the choice of operating variables to ensure operation in a single supercritical phase. Kordikowski et al.[84] studied the volume expansion and vapor-liquid equilibrium properties of CO_2, ethane, and ethylene binary mixtures with polar solvents. From this data, the binary interaction parameter (k_{ij}) was regressed and fit using the Peng-Robinson equation of state[109] with van der Waals mixing in Aspen Plus (Version 11). The experimental bubble point data and Peng-Robinson model predictions are plotted in Figure 3.10. The regressed binary interaction parameter for ethylene-EtOAc was k_{ij} = -0.0356 and the model fit had an R^2 value of 0.9887.

Using the fitted interaction parameter, more simulations of the ethylene-EtOAc system were done to determine its critical loci at all temperatures and compositions. The critical loci

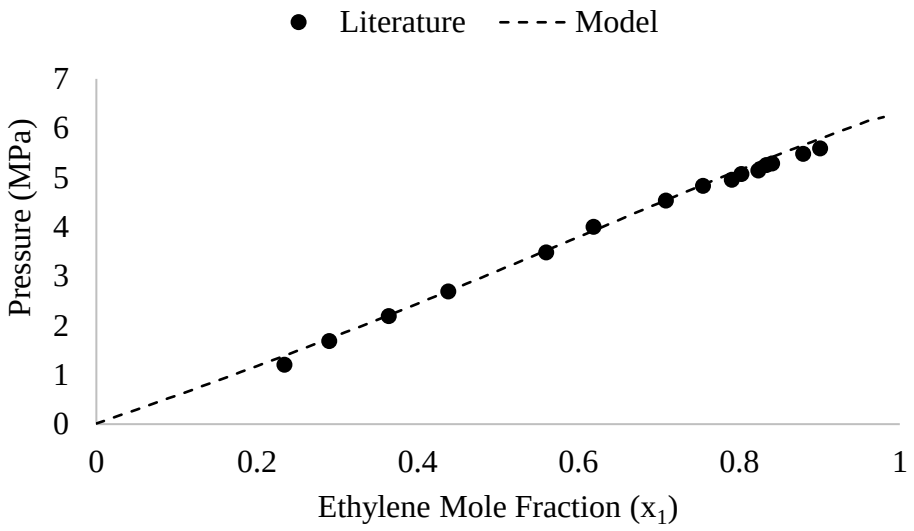

Figure 3.9: Ethylene (x) – EtOAc (x_2) system at 25°C modelled with the Peng-Robinson equation of state using the regressed binary interaction parameters from the plotted literature data.

were modelled using the Peng-Robinson equation of state and solved using the method outlined by Deiters and Bell.[89] The behavior of the modelled binary SC system is Type 1[87] as shown in Figure 3.11. Thus, the binary system will be supercritical at all compositions if the operating temperature and pressure are above the maximum of the critical loci. At an operating temperature of 20°C, the system will be in a single supercritical phase at all compositions above 5.84 MPa and should enable precipitation of dissolved vanillin and *p*HB.

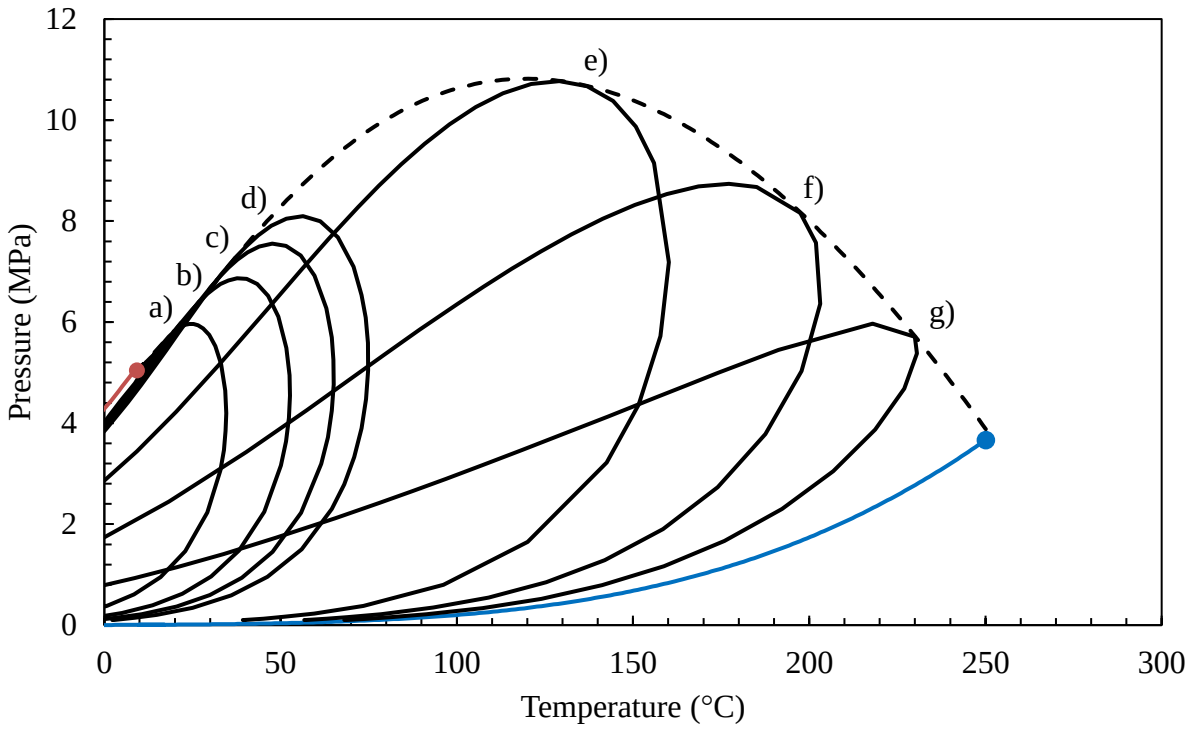

Figure 3.10: Mixture critical loci for ethylene-ethyl acetate with curves for a)-g) 0.01, 0.02, 0.03, 0.04, 0.25, 0.5, 0.75 mol fraction ethyl acetate (x_2). Colored line represents pure vapor pressure, colored dot is the pure critical point, red = ethylene, blue = ethyl acetate

3.3.5 Vanillin Precipitation with Supercritical Ethylene as Antisolvent

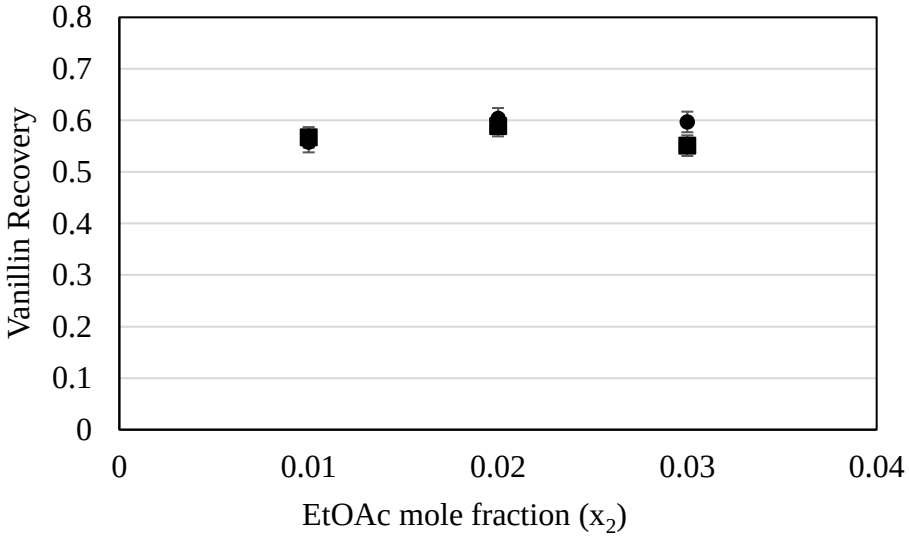

Figure 3.11: Recoveries of vanillin from *sc*C_2H_4 (x_1) at 20°C and various organic solvent mole fractions (x_2). Experimental pressures: 8.27 MPa (■), 7.58 MPa (●)

Ethylene was chosen as the final SCF because it has a low T_c (9.19°C), relative to CO_2 and ethane, and is food grade. As there exist sparse reported phase behavior information for the binary ethylene-EtOAc system, the system was modelled as explained in Section 3.5. The yield of precipitated vanillin was the highest (60.4 ± 0.2%) when using ethylene as the SCF antisolvent. The operating conditions to maintain a supercritical phase of the organic solvent+SCF antisolvent binary system are listed in Table 3.2. The improved yield implies that temperature of the system has the greatest effect on recovery, due to the reduced vapor pressure of vanillin and *p*HB. Experiments at sub-ambient temperatures would likely show even greater recoveries.

Table 3.2: Optimum SCF Experimental Parameters for Ethylene

Parameter	*Value*
Temperature	20.0°C
Pressure	7.58 MPa
Mole Fraction EtOAc	0.02
Vessel Volume	300 mL
Spray Rate	3.0 ± 0.1 mL/min
Solution Volume	12.0 ± 0.1 mL
Solute Concentration	200.0 ± 0.5 mg/mL
Impeller Speed	1000 ± 20 RPM
Wash Time	60 min

3.4 Optimizing Recoveries of Organic Solvent and Precipitated Product

3.4.1 Solvent Recovery

Assuming that the vessel is perfectly mixed during the solvent flush phase (post spraying), a flush time equivalent to six residence times was chosen for the SCF solvent at the crystallization pressure and temperature (Equation 3.1). Based on this calculation, 30 mL/min of SCF at the operating P and T was flowed for 60 minutes to remove nearly all solvent. The predicted effect of SCF wash flow rate on the concentration of the oganic solvent in the effluent is plotted in Figure 3.12. Having a sufficiently long wash time (~ six residence times) should lead to complete removal of co-solvent from the precipitation vessel, leaving a dry powder.

$$C = C_o\left(1 - e^{\frac{-t}{\tau}}\right), C_o = Initial\ Concentration, \tau = Residence\ Time, t = time \quad (Eq\ 3.1)$$

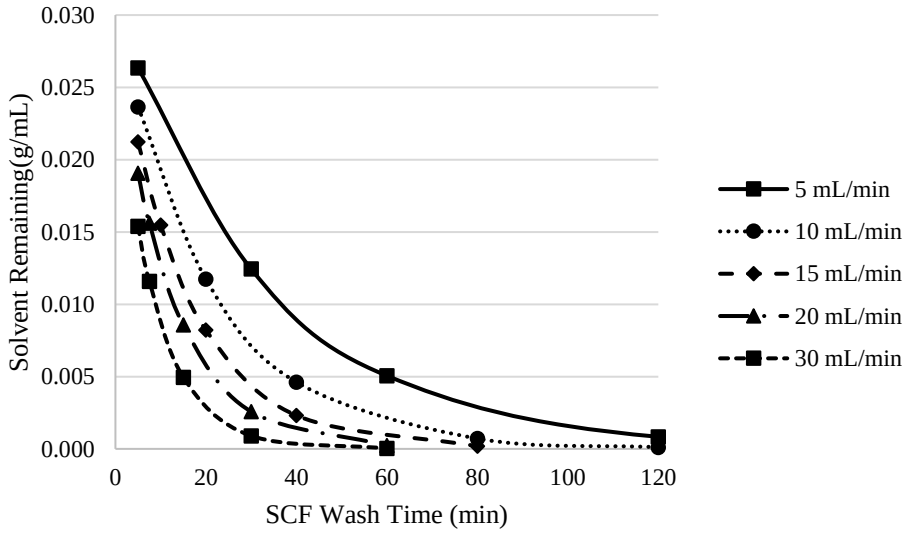

Figure 3.12: Effluent solvent concentration as a function of wash time and SCF flow rate, modelled using a differential mass balance.

Collecting the used organic solvent from the effluent stream proved to be a challenge. Early experiments consistently showed less than 50% recovery based on mass balance calculations. Initially, the organic solvent was collected intermittently from the condenser during

the solvent wash cycle to reduce loss by evaporation. The condenser also cooled to -10°C but this only marginally improved solvent recovery. Hence, the volume of the solvent collection reservoir was increased from 125 mL to 1 L with a dip tube. These modifications increased the organic solvent recovery from approximately 50% to an average of 79.9 ± 1.1 % over 4 consecutive experiments.

3.4.2 Optimized Recoveries of Vanillin and *p*HB

The recovery of vanillin from the reactor was 60.4 ± 1.2 % in the first experiments involving supercritical ethylene. Using the equation of state model, it was determined that use of a lower pressure in the SAS process would likely improve vanillin recovery in the vessel by reducing the SCF mixture's ability to dissolve vanillin. Accordingly, a reduced pressure of 6.90 MPa that was sufficiently above the mixture critical point at 20°C and $x_{EtOAc} = 0.02$ was chosen. At these conditions 74.8 ± 0.9 % of vanillin was recovered as a solid in the precipitation vessel and 79.3 ± 0.2 % of EtOAc was recovered from the condenser.

Table 3.3: Optimized Conditions for Vanillin Precipitation

Parameter	***Value***
Pressure	6.90 ± 0.21 MPa
Temperature	20.0 ± 1.0 °C
Vanillin concentration in spray solution	200.0 ± 0.5 mg/mL
Spray Rate	3.0 ± 0.1 ml/min
Spray Time	120 s
Impeller Speed	1000 ± 20 RPM
Wash Phase	60 min @ 30.0 ± 0.1 ml/min of SCF at 6.90 MPa and 20 °C

To precipitate *p*HB, several different pressures were used starting with the optimized conditions for vanillin precipitation. *p*HB precipitated at all pressures above the mixture critical point. However, the highest recovery achieved (50.8 ± 1.4%) was much lower than vanillin. The

lower recovery is likely due to *p*HB being more polar and more soluble in the SCF+EtOAc mixture.

Table 3.4: Recovery of pHB From Various Pressures of C_2H_4

Pressure (MPa)	*p*HB Sprayed (g)	*p*HB Recovery (%)
6.90	0.525 ± 0.002	50.8 ± 1.4
7.58	0.762 ± 0.002	47.2 ± 1.5
8.27	0.845 ± 0.002	44.3 ± 1.5
8.96	0.918 ± 0.001	42.9 ± 1.5
9.65	0.990 ± 0.001	40.2 ± 1.5

To determine where loss of products is occurring, the crystallization equipment used was cleaned and analyzed by GC-FID to investigate residual vanillin along with the collected solvent. Due to vanillin dissolving and exiting the crystallizer, the equipment immediately after the crystallizer contained 10.3 ± 0.1% of the total vanillin sprayed into the vessel. The recovered solvent also contained 9.4 ± 0.2% of the total vanillin bringing vanillin's mass balance to 94.5 ± 0.3 %. The missing product is assumed to have been carried away in the gas outlet.

To examine the potential for mass transfer limitations within this system, studies were done using the ultrasonic VibraCell. EtOAc containing vanillin was loaded in the cell and pressurized with ethylene using the optimized conditions above. The ultrasonic wand was pulsed for several minutes during the wash cycle to break up any potential droplets of solvent that had not formed a continuous phase with the SCF. The average vanillin recovery from this was 62.8 ± 2.4% which was comparable to the vanillin recoveries obtained with impeller mixing. Ultrasonic nozzles have been used for SAS processes to enhance mass transfer rates between the organic solvent and SCF phase by creating smaller droplets of the solution.[110] However, ultrasonic

mixing did not improve the recovery of vanillin suggesting that vapor pressure effects likely dominate the vanillin recovery.

3.5 Solids Analysis

The recovered precipitates were analyzed using Differential Scanning Calorimetry (DSC) to determine their melting profiles. Any significant change in the melting point range could mean that the precipitate is not pure and contains contaminants such as solvent or other impurities. As inferred from Figures 3.13 And 3.14, the DSC profiles of precipitated vanillin and *p*HB closely match their standards indicating that there is little contamination or modification as a result of the SAS processing. The vanillin standard had a melting point (MP) of 82.77 ± 0.02°C, the SAS precipitated vanillin had a MP of 82.62 ± 0.02°C. The *p*HB standard had a MP of 117.16 ± 0.01°C, and the SAS precipitate had a MP of 116.52 ± 0.01°C. See Appendix D for SEM images of the micronized solute particles.

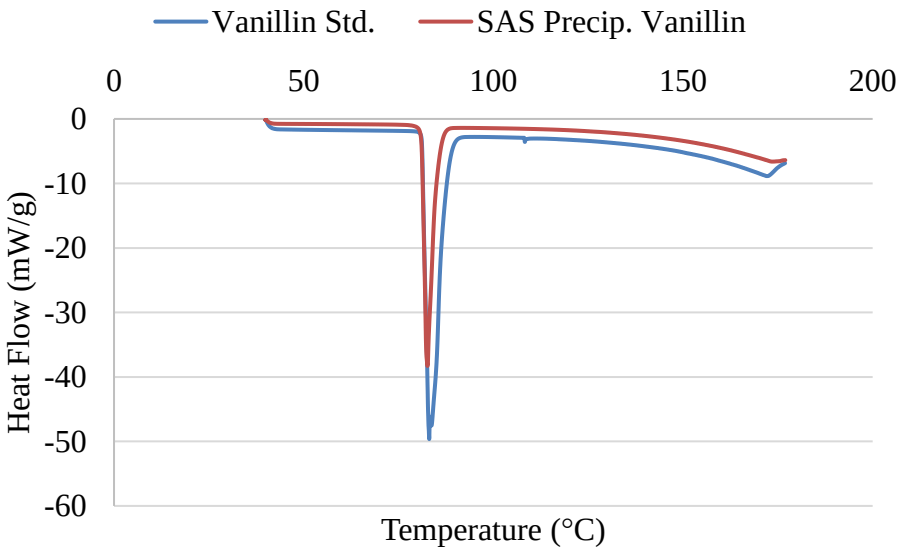

Figure 3.13: The melting point profile of vanillin standard and SAS precipitate. Heating rate of 10°C/min.

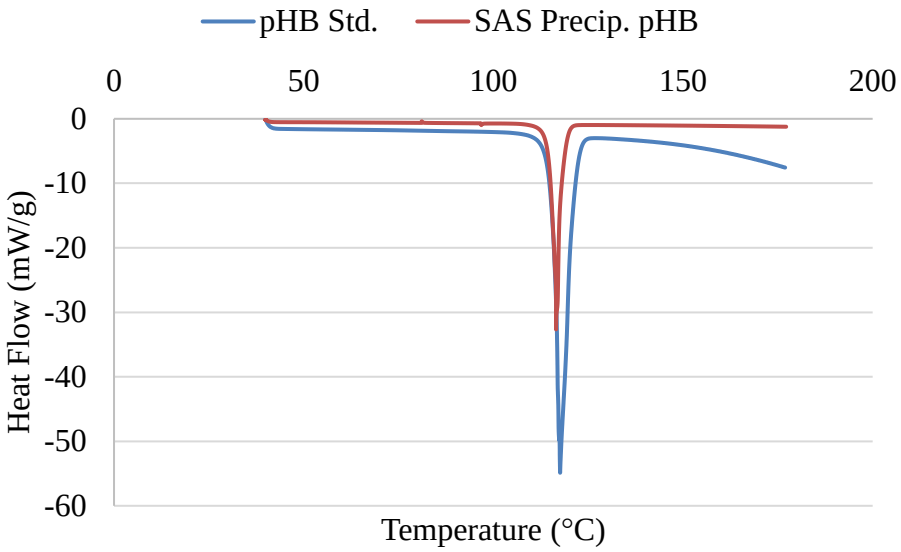

Figure 3.14: The melting point profiles of *p*HB standard and SAS precipitate. Heating rate of 10°C/min.

In summary, a rapid supercritical antisolvent process was demonstrated for recrystallizing vanillin and *p*HB from their solutions. However, the yields of the crystallized solids recovered in the vessel can be improved by further optimization of reactor operating conditions and choice of the SCF solvent and organic solvent. Further, the recovery of the organic solvent along with the dissolved solute that escapes the crystallizer must also be maximized to favor process economics.

4 Conclusions and Recommendations

4.1 Conclusions

Technology concepts for separating vanillin and *p*-hydroxybenzaldehyde (*p*HB) from the LMW fraction of ozonized corn lignin were successfully developed and demonstrated using chromatography and rapid crystallization using the supercritical antisolvent process (SAS).

Chromatography was successfully shown to separate model mixtures of vanillin and *p*HB utilizing a step gradient of 15% acetic acid (AcOH) in toluene to 45% AcOH in toluene, following complete elution of only vanillin. The column utilized a 500 mL bed of silica gel-60 to partition vanillin and *p*HB by polarity, successfully recovering 98.5 ± 2.0% of vanillin and 91.1 ± 1.3% of *p*HB. The overall mass balance including the mobile phase was 97.2 ± 0.9%. Utilizing the step gradient greatly increased the speed and the extent of recovery of *p*HB with excellent separation of the solutes. The developed method was shown to separate vanillin and *p*HB extracted from ozonized corn cob lignin solution.

SAS process using supercritical ethylene at room temperature and mild pressure of 6.9 MPa shows promise for rapidly crystallizing vanillin and *p*HB from their respective solutions in ethyl acetate. Spraying either vanillin or *p*HB solution into supercritical ethylene causes rapid absorption of the solvent from the droplets into the supercritical fluid (SCF) leaving a dry crystalline powder. The recovery of vanillin and *p*HB was optimized by tuning the pressure of the vessel and the flow rate of the SCF during the drying step. The maximum solute recoveries demonstrated were 74.8 ± 0.9 % for vanillin and 50.8 ± 1.4% for *p*HB in the vessel. Approximately 19.4% of vanillin was recovered from the condensed organic solvent showing that a significant amount dissolved into the SCF+solvent phase but could be recycled along with

the solvent. Based on DSC results, the obtained SAS precipitates of vanillin and *p*HB had little change in purity after recrystallization.

These results show that vanillin and *p*HB could be separated by chromatography from a depolymerized lignin mixture and then crystallized using SAS in a continuous process. This new process shows promise for achieving the difficult separation of value-added aldehydes from lignin.

4.2 Recommendations

The results from this work pave the way for further work aimed at optimizing the chromatography and crystallization techniques. Specific recommendations include the following:

1. The step gradient chromatography should be run with LMW extracts of ozonized corn cob lignin solution to establish quantitative separations of the vanillin and *p*HB containing fractions for further processing.
2. The concentrations of vanillin and *p*HB in the supercritical SCF+solvent system at operating conditions should be measured by experimental methods (on-line GC) to enable mass balance closure and rationally guide further process optimization (choice of P, T, co-solvent, enhanced mixing, etc.)
3. Perform SAS using ethylene at sub-ambient supercritical temperatures to assess the impact on vanillin and *p*HB yields as dry powders.
4. Investigate alcohol-ethyl acetate solvent systems for use in resin chromatography based on recent literature,[111] using food grade solvents. Using as much of the same solvents for extraction of the LMW compounds and for separating them is ideal to reduce energy and solvent costs.

5. Investigate the solubility of acetic acid and toluene in SCF so that the separated *p*HB and vanillin streams from column chromatography can be directly processed.
6. Investigate the transition from flash chromatography to simulated moving bed (SMB) chromatography. This system is especially well suited for SMB because it is a binary separation. This will allow vanillin and *p*HB to be continuously separated and may allow the use of alternate solvent systems.
7. Perform an economic and environmental impact analyses of the combined chromatography and SAS processes, based on the data acquired to date, to identify hotspots and to guide process design and development.

References

(1) Han, J. *What is Vanillin in Food? Types, Production, Uses, and Differences with Vanilla extract*. https://foodadditives.net/flavors/vanillin/ (accessed 2022-06-02).

(2) Fache, M.; Boutevin, B.; Caillol, S. Vanillin Production from Lignin and Its Use as a Renewable Chemical. *ACS Sustain. Chem. Eng.* **2016**, *4* (1), 35–46. https://doi.org/10.1021/acssuschemeng.5b01344.

(3) Mordor Intellignece. *Vanillin Market | 2022 - 27 | Industry Share, Size, Growth - Mordor Intelligence*. Mordor Intelligence. https://www.mordorintelligence.com/industry-reports/vanillin-market (accessed 2022-06-02).

(4) Ciriminna, R.; Fidalgo, A.; Meneguzzo, F.; Parrino, F.; Ilharco, L. M.; Pagliaro, M. Vanillin: The Case for Greener Production Driven by Sustainability Megatrend. *ChemistryOpen* **2019**, *8* (6), 660–667. https://doi.org/10.1002/open.201900083.

(5) Martău, G. A.; Călinoiu, L.-F.; Vodnar, D. C. Bio-Vanillin: Towards a Sustainable Industrial Production. *Trends Food Sci. Technol.* **2021**, *109*, 579–592. https://doi.org/10.1016/j.tifs.2021.01.059.

(6) United States Department of Agriculture. *Corn and soybean production up in 2021, USDA Reports Corn and soybean stocks up from year earlier, Winter Wheat Seedings up for 2022*. USDA National Agricultural Statistics Service. https://www.nass.usda.gov/Newsroom/2022/01-12-2022.php (accessed 2022-06-02).

(7) Koundinya, V. *Corn Stover*. Ag Marketing Resource Center. https://www.agmrc.org/commodities-products/biomass/corn-stover (accessed 2022-06-02).

(8) United States Department of Agriculture. *USDA/NASS 2021 State Agriculture Overview for Kansas*. USDA National Agricultural Statistics Service. https://www.nass.usda.gov/Quick_Stats/Ag_Overview/stateOverview.php?state=KANSAS (accessed 2022-06-02).

(9) Mayer, M. *Value of Corn Stover*. University of Wisconsin Green County Extension. https://green.extension.wisc.edu/files/2010/05/Corn-stalk-value-2017.pdf (accessed 2022-05-19).

(10) Jiang, Z.; Hu, C. Selective Extraction and Conversion of Lignin in Actual Biomass to Monophenols: A Review. *J. Energy Chem.* **2016**, *25* (6), 947–956. https://doi.org/10.1016/j.jechem.2016.10.008.

(11) Ponnusamy, V. K.; Nguyen, D. D.; Dharmaraja, J.; Shobana, S.; Banu, J. R.; Saratale, R. G.; Chang, S. W.; Kumar, G. A Review on Lignin Structure, Pretreatments, Fermentation Reactions and Biorefinery Potential. *Bioresour. Technol.* **2019**, *271*, 462–472. https://doi.org/10.1016/j.biortech.2018.09.070.

(12) Hong, S.-H.; Hwang, S.-H. A Concise Review of Recent Application Progress and Future Prospects for Lignin as Biomass Utilization. *Elastomers Compos.* **2021**, *56* (3), 136–151. https://doi.org/10.7473/EC.2021.56.3.136.

(13) Gioia, C.; Colonna, M.; Tagami, A.; Medina, L.; Sevastyanova, O.; Berglund, L. A.; Lawoko, M. Lignin-Based Epoxy Resins: Unravelling the Relationship between Structure and Material Properties. *Biomacromolecules* **2020**, *21* (5), 1920–1928. https://doi.org/10.1021/acs.biomac.0c00057.

(14) Silverman, J. R.; Danby, A. M.; Subramaniam, B. Facile Prepolymer Formation with Ozone-Pretreated Grass Lignin by In Situ Grafting of Endogenous Aromatics. *ACS*

Sustain. Chem. Eng. **2020**, *8* (46), 17001–17007. https://doi.org/10.1021/acssuschemeng.0c03811.

(15) Silva, E. A. B. da; Zabkova, M.; Araújo, J. D.; Cateto, C. A.; Barreiro, M. F.; Belgacem, M. N.; Rodrigues, A. E. An Integrated Process to Produce Vanillin and Lignin-Based Polyurethanes from Kraft Lignin. *Chem. Eng. Res. Des.* **2009**, *87* (9), 1276–1292. https://doi.org/10.1016/j.cherd.2009.05.008.

(16) Wongtanyawat, N.; Lusanandana, P.; Khwanjaisakun, N.; Kongpanna, P.; Phromprasit, J.; Simasatitkul, L.; Amornraksa, S.; Assabumrungrat, S. Comparison of Different Kraft Lignin-Based Vanillin Production Processes. *Comput. Chem. Eng.* **2018**, *117*, 159–170. https://doi.org/10.1016/j.compchemeng.2018.05.020.

(17) R. Silverman, J.; M. Danby, A.; Subramaniam, B. Intensified Ozonolysis of Lignins in a Spray Reactor: Insights into Product Yields and Lignin Structure. *React. Chem. Eng.* **2019**, *4* (8), 1421–1430. https://doi.org/10.1039/C9RE00098D.

(18) Danby, A. M.; Lundin, M. D.; Subramaniam, B. Valorization of Grass Lignins: Swift and Selective Recovery of Pendant Aromatic Groups with Ozone. *ACS Sustain. Chem. Eng.* **2018**, *6* (1), 71–76. https://doi.org/10.1021/acssuschemeng.7b02978.

(19) Santos, R. B.; Capanema, E. A.; Balakshin, M. Yu.; Chang, H.; Jameel, H. Lignin Structural Variation in Hardwood Species. *J. Agric. Food Chem.* **2012**, *60* (19), 4923–4930. https://doi.org/10.1021/jf301276a.

(20) Li, M.; Foster, C.; Kelkar, S.; Pu, Y.; Holmes, D.; Ragauskas, A.; Saffron, C. M.; Hodge, D. B. Structural Characterization of Alkaline Hydrogen Peroxide Pretreated Grasses Exhibiting Diverse Lignin Phenotypes. *Biotechnol. Biofuels* **2012**, *5* (1), 38. https://doi.org/10.1186/1754-6834-5-38.

(21) Mota, M. Fractionation and Purification of Syringaldehyde and Vanilin from Oxidation of Lignin, Universidade do Porto, 2017.

(22) Hodásová, Ľ.; Jablonsky, M.; Butor Skulcova, A.; Haz, A. Lignin, Potential Products and Their Market Value. *Wood Res.* **2015**, *60*, 973–986.

(23) Havkin-Frenkel, D. Vanillin. In *Kirk-Othmer Encyclopedia of Chemical Technology*; John Wiley & Sons, Ltd, 2018; pp 1–12. https://doi.org/10.1002/0471238961.2201140905191615.a01.pub3.

(24) Maliverney, C.; Mulhauser, M. Hydroxybenzaldehydes. In *Kirk-Othmer Encyclopedia of Chemical Technology*; John Wiley & Sons, Ltd, 2000. https://doi.org/10.1002/0471238961.0825041813011209.a01.

(25) PEARL, I. A. SILVER CATALYZED REACTIONS OF PHENOLIC ALDEHYDES1. *J. Org. Chem.* **1947**, *12* (1), 85–89. https://doi.org/10.1021/jo01165a012.

(26) Ma, Y.; Teng, B.; Cao, L.; Zhong, D.; Ji, S.; Teng, F.; Liu, J.; Yao, Y.; Tang, J.; Tong, J. Growth, Structural, Thermal, Dielectric and Optical Studies on HBST Crystal: A Potential THz Emitter. *Spectrochim. Acta. A. Mol. Biomol. Spectrosc.* **2018**, *190*, 274–282. https://doi.org/10.1016/j.saa.2017.08.035.

(27) Mota, M. I. F.; Rodrigues Pinto, P. C.; Loureiro, J. M.; Rodrigues, A. E. Recovery of Vanillin and Syringaldehyde from Lignin Oxidation: A Review of Separation and Purification Processes. *Sep. Purif. Rev.* **2016**, *45* (3), 227–259. https://doi.org/10.1080/15422119.2015.1070178.

(28) Schaefer, B. *Natural Products in the Chemical Industry*; Springer, 2015.

(29) Ward, D. Scalable Separation Methods for the Isolation of Monosaccharides in a Biorefinery Context. Doctoral, UCL (University College London), 2018.

(30) Mota, I. F.; Pinto, P. R.; Loureiro, J. M.; Rodrigues, A. E. Purification of Syringaldehyde and Vanillin from an Oxidized Industrial Kraft Liquor by Chromatographic Processes. *Sep. Purif. Technol.* **2020**, *234*, 116083. https://doi.org/10.1016/j.seppur.2019.116083.
(31) Gallagher, P. M.; Coffey, M. P.; Krukonis, V. J.; Klasutis, N. Gas Antisolvent Recrystallization: New Process To Recrystallize Compounds Insoluble in Supercritical Fluids. In *Supercritical Fluid Science and Technology*; Johnston, K. P., Penninger, J. M. L., Eds.; ACS Symposium Series; American Chemical Society: Washington, DC, 1989; Vol. 406, pp 334–354. https://doi.org/10.1021/bk-1989-0406.ch022.
(32) Kathahira, R.; Elder, T. J.; Beckham, G. T. A Brief Introduction to Lignin Structure. *Lignin Valorization Emerg. Approaches Energy Environ. Ser. No 19* **2018**, *19*, 1–20. https://doi.org/10.1039/9781788010351-00001.
(33) Almeida, A. R. R. P.; Freitas, V. L. S.; Campos, J. I. S.; Ribeiro da Silva, M. D. M. C.; Monte, M. J. S. Volatility and Thermodynamic Stability of Vanillin. *J. Chem. Thermodyn.* **2019**, *128*, 45–54. https://doi.org/10.1016/j.jct.2018.07.023.
(34) Khwanjaisakun, N.; Amornraksa, S.; Simasatitkul, L.; Charoensuppanimit, P.; Assabumrungrat, S. Techno-Economic Analysis of Vanillin Production from Kraft Lignin: Feasibility Study of Lignin Valorization. *Bioresour. Technol.* **2020**, *299*, 122559. https://doi.org/10.1016/j.biortech.2019.122559.
(35) Green, M. *Solvay increases natural vanillin production amid heightened market demand*. Food Ingredients First. https://www.foodingredientsfirst.com/news/solvay-increases-natural-vanillin-production-amid-heightened-market-demand.html (accessed 2022-05-26).
(36) Vibert, M.; Cochennec, C.; Etchebarne, A. Method for Purifying Vanillin by Liquid-Liquid Extraction. US9126917B2, September 8, 2015.
(37) Sandborn, L. T.; Richter, S. J.; Clemens, H. G. Process of Making Vanillin. US2057117A, October 13, 1936.
(38) Rødsrud, G.; Lersch, M.; Sjöde, A. History and Future of World's Most Advanced Biorefinery in Operation. *Biomass Bioenergy* **2012**.
(39) Evju, H. Process for Preparation of 3-Methoxy-4-Hydroxybenzaldehyde. US4151207A, April 24, 1979.
(40) Płotka, J.; Tobiszewski, M.; Sulej, A. M.; Kupska, M.; Górecki, T.; Namieśnik, J. Green Chromatography. *J. Chromatogr. A* **2013**, *1307*, 1–20. https://doi.org/10.1016/j.chroma.2013.07.099.
(41) Schmidt-Traub, H.; Schulte, M.; Seidel-Morgenstern, A. *Preparative Chromatography*; John Wiley & Sons, 2020.
(42) Watson, J. T.; Sparkman, O. D. *Introduction to Mass Spectrometry: Instrumentation, Applications, and Strategies for Data Interpretation*; John Wiley & Sons, 2007.
(43) Collin, S.; Nizet, S.; Claeys Bouuaert, T.; Despatures, P.-M. Main Odorants in Jura Flor-Sherry Wines. Relative Contributions of Sotolon, Abhexon, and Theaspirane-Derived Compounds. *J. Agric. Food Chem.* **2012**, *60* (1), 380–387. https://doi.org/10.1021/jf203832c.
(44) Vempatapu, B. P.; Kumar, J.; Ray, A.; Chhibber, V. K.; Kanaujia, P. K. Determination of Biodiesel and Used Cooking Oil in Automotive Diesel/Green Diesel Fuels through High-Performance Liquid Chromatography. *J. Chromatogr. A* **2020**, *1629*, 461512. https://doi.org/10.1016/j.chroma.2020.461512.
(45) Johnson, C. B.; Kazantzis, A.; Skoula, M.; Mitteregger, U.; Novak, J. Seasonal, Populational and Ontogenic Variation in the Volatile Oil Content and Composition of

Individuals of Origanum Vulgare Subsp. Hirtum, Assessed by GC Headspace Analysis and by SPME Sampling of Individual Oil Glands. *Phytochem. Anal.* **2004**, *15* (5), 286–292. https://doi.org/10.1002/pca.780.

(46) A.G.Huesgen. *Analysis of natural and artificial vanilla preparations*. Agilent Application Solution. https://www.agilent.com/cs/library/slidepresentation/Public/Natural_and_Artificial_Vanilla.pdf (accessed 2022-06-06).

(47) Fair, J. D.; Kormos, C. M. Flash Column Chromatograms Estimated from Thin-Layer Chromatography Data. *J. Chromatogr. A* **2008**, *1211* (1), 49–54. https://doi.org/10.1016/j.chroma.2008.09.085.

(48) Hofmeister, G.; Alberg, D.; Mohrig, J. R.; Hammond, C. N.; Schatz, P. F. *Laboratory Techniques in Organic Chemistry*; Macmillan Learning, 2014.

(49) Silver, J. Let Us Teach Proper Thin Layer Chromatography Technique! *J. Chem. Educ.* **2020**, *97* (12), 4217–4219. https://doi.org/10.1021/acs.jchemed.0c00437.

(50) Coskun, O. Separation Techniques: Chromatography. *North. Clin. Istanb.* **2016**, *3* (2), 156–160. https://doi.org/10.14744/nci.2016.32757.

(51) Hanai, T. Fundamental Properties of Packing Materials for Liquid Chromatography. *Separations* **2019**, *6* (1), 2. https://doi.org/10.3390/separations6010002.

(52) Gomes, E. D.; Mota, M. I.; Rodrigues, A. E. Fractionation of Acids, Ketones and Aldehydes from Alkaline Lignin Oxidation Solution with SP700 Resin. *Sep. Purif. Technol.* **2018**, *194*, 256–264. https://doi.org/10.1016/j.seppur.2017.11.050.

(53) Gomes, E. D.; Rodrigues, A. E. Lignin Biorefinery: Separation of Vanillin, Vanillic Acid and Acetovanillone by Adsorption. *Sep. Purif. Technol.* **2019**, *216*, 92–101. https://doi.org/10.1016/j.seppur.2019.01.071.

(54) Vigneault, A.; Johnson, D. K.; Chornet, E. Base-Catalyzed Depolymerization of Lignin: Separation of Monomers. *Can. J. Chem. Eng.* **2007**, *85* (6), 906–906.

(55) Zhao, Y.; Ouyang, X.; Chen, J.; Zhao, L.; Qiu, X. Separation of Aromatic Monomers from Oxidatively Depolymerized Products of Lignin by Combining Sephadex and Silica Gel Column Chromatography. *Sep. Purif. Technol.* **2018**, *191*, 250–256. https://doi.org/10.1016/j.seppur.2017.09.039.

(56) Kromidas, S. 1.2 Special Features of the Gradient. In *Gradient HPLC for Practitioners - RP, LC-MS, Ion Analytics, Biochromatography, SFC, HILIC*; John Wiley & Sons, 2019.

(57) Broeckhoven, K.; Desmet, G. Theory of Separation Performance and Peak Width in Gradient Elution Liquid Chromatography: A Tutorial. *Anal. Chim. Acta* **2022**, 339962. https://doi.org/10.1016/j.aca.2022.339962.

(58) Subramaniam, B.; Rajewski, R. A.; Snavely, K. Pharmaceutical Processing with Supercritical Carbon Dioxide. *J. Pharm. Sci.* **1997**, *86* (8), 885–890. https://doi.org/10.1021/js9700661.

(59) Phelps, C. L.; Smart, N. G.; Wai, C. M. Past, Present, and Possible Future Applications of Supercritical Fluid Extraction Technology. *J. Chem. Educ.* **1996**, *73* (12), 1163. https://doi.org/10.1021/ed073p1163.

(60) Kulazynski, M.; Stolarski, M.; Faltynowicz, H.; Narowska, B.; Swiatek, L.; Lukaszewicz, M. Supercritical Fluid Extraction of Vegetable Materials. *Chem. Chem. Technol.* **2016**, *10* (4s), 637–643. https://doi.org/10.23939/chcht10.04si.637.

(61) Saito, M. History of Supercritical Fluid Chromatography: Instrumental Development. *J. Biosci. Bioeng.* **2013**, *115* (6), 590–599. https://doi.org/10.1016/j.jbiosc.2012.12.008.

(62) Harjo, B.; Ng, K. M.; Wibowo, C. Synthesis of Supercritical Crystallization Processes. *Ind. Eng. Chem. Res.* **2005**, *44* (22), 8248–8259. https://doi.org/10.1021/ie050791j.
(63) Reverchon, E. Supercritical Antisolvent Precipitation of Micro- and Nano-Particles. *J. Supercrit. Fluids* **1999**, *15* (1), 1–21. https://doi.org/10.1016/S0896-8446(98)00129-6.
(64) Muhrer, G.; Lin, C.; Mazzotti, M. Modeling the Gas Antisolvent Recrystallization Process. *Ind. Eng. Chem. Res.* **2002**, *41* (15), 3566–3579. https://doi.org/10.1021/ie020070+.
(65) Fusaro, F.; Mazzotti, M.; Muhrer, G. Gas Antisolvent Recrystallization of Paracetamol from Acetone Using Compressed Carbon Dioxide as Antisolvent. *Cryst. Growth Des.* **2004**, *4* (5), 881–889. https://doi.org/10.1021/cg034172u.
(66) Huang, J.; Moriyoshi, T. Fabrication of Fine Powders by RESS with a Clearance Nozzle. *J. Supercrit. Fluids* **2006**, *37* (3), 292–297. https://doi.org/10.1016/j.supflu.2005.11.024.
(67) Cuadra, I. A.; Cabañas, A.; Cheda, J. A. R.; Martínez-Casado, F. J.; Pando, C. Pharmaceutical Co-Crystals of the Anti-Inflammatory Drug Diflunisal and Nicotinamide Obtained Using Supercritical CO2 as an Antisolvent. *J. CO2 Util.* **2016**, *13*, 29–37. https://doi.org/10.1016/j.jcou.2015.11.006.
(68) FDA. *CFR - Code of Federal Regulations Title 21*; 2008.
(69) Yaws, C. L. *Yaws' Critical Property Data for Chemical Engineers and Chemists*; Knovel, 2014.
(70) Klemola, A.; Tuovinen, J. Method for the Production of Vanillin. US4847422A, July 11, 1989.
(71) Numan-Al-Mobin, A. M.; Kolla, P.; Dixon, D.; Smirnova, A. Effect of Water–Carbon Dioxide Ratio on the Selectivity of Phenolic Compounds Produced from Alkali Lignin in Sub- and Supercritical Fluid Mixtures. *Fuel* **2016**, *185*, 26–33. https://doi.org/10.1016/j.fuel.2016.07.043.
(72) Escobar, E. L. N.; da Silva, T. A.; Pirich, C. L.; Corazza, M. L.; Pereira Ramos, L. Supercritical Fluids: A Promising Technique for Biomass Pretreatment and Fractionation. *Front. Bioeng. Biotechnol.* **2020**, *8*.
(73) Jin, J.; Wang, Y.; Zhang, H.; Fan, X.; Wu, H. Solubility of 4-Hydroxybenzaldehyde in Supercritical Carbon Dioxide with and without Cosolvents. *J. Chem. Eng. Data* **2014**, *59* (5), 1521–1527. https://doi.org/10.1021/je401082x.
(74) Mao, H.; Chen, H.; Jin, M.; Wang, C.; Xiao, Z.; Niu, Y. Measurement and Correlation of Solubility of O-Vanillin in Different Pure and Binary Solvents at Temperatures from 273.15 K to 303.15 K. *J. Chem. Thermodyn.* **2020**, *150*, 106199. https://doi.org/10.1016/j.jct.2020.106199.
(75) Murga, R.; Sanz, M. T.; Beltrán, S.; Cabezas, J. L. Solubility of Syringic and Vanillic Acids in Supercritical Carbon Dioxide. *J. Chem. Eng. Data* **2004**, *49* (4), 779–782. https://doi.org/10.1021/je034129a.
(76) Rojas-Ávila, A.; Pimentel-Rodas, A.; Rosales-García, T.; Dávila-Ortiz, G.; Galicia-Luna, L. A. Solubility of Binary and Ternary Systems Containing Vanillin and Vanillic Acid in Supercritical Carbon Dioxide. *J. Chem. Eng. Data* **2016**, *61* (9), 3225–3232. https://doi.org/10.1021/acs.jced.6b00322.
(77) Montes, A.; Merino, R.; De los Santos, D. M.; Pereyra, C.; Martínez de la Ossa, E. J. Micronization of Vanillin by Rapid Expansion of Supercritical Solutions Process. *J. CO2 Util.* **2017**, *21*, 169–176. https://doi.org/10.1016/j.jcou.2017.07.009.

(78) Myint, A. A.; Lee, H. W.; Seo, B.; Son, W.-S.; Yoon, J.; Yoon, T. J.; Park, H. J.; Yu, J.; Yoon, J.; Lee, Y.-W. One Pot Synthesis of Environmentally Friendly Lignin Nanoparticles with Compressed Liquid Carbon Dioxide as an Antisolvent. *Green Chem.* **2016**, *18* (7), 2129–2146. https://doi.org/10.1039/C5GC02398J.

(79) Haghbakhsh, R.; Hayer, H.; Saidi, M.; Keshtkari, S.; Esmaeilzadeh, F. Density Estimation of Pure Carbon Dioxide at Supercritical Region and Estimation Solubility of Solid Compounds in Supercritical Carbon Dioxide: Correlation Approach Based on Sensitivity Analysis. *Fluid Phase Equilibria* **2013**, *342*, 31–41. https://doi.org/10.1016/j.fluid.2012.12.029.

(80) Kankala, R. K.; Zhang, Y. S.; Wang, S.-B.; Lee, C.-H.; Chen, A.-Z. Supercritical Fluid Technology: An Emphasis on Drug Delivery and Related Biomedical Applications. *Adv. Healthc. Mater.* **2017**, *6* (16), 10.1002/adhm.201700433. https://doi.org/10.1002/adhm.201700433.

(81) Branch, J. A.; Bartlett, P. N. Electrochemistry in Supercritical Fluids. *Philos. Trans. R. Soc. Math. Phys. Eng. Sci.* **2015**, *373* (2057), 20150007. https://doi.org/10.1098/rsta.2015.0007.

(82) Subramaniam, B.; McHugh, M. A. Reactions in Supercritical Fluids - a Review. *Ind. Eng. Chem. Process Des. Dev.* **1986**, *25* (1), 1–12. https://doi.org/10.1021/i200032a001.

(83) Olmos, A.; Asensio, G.; Pérez, P. J. Homogeneous Metal-Based Catalysis in Supercritical Carbon Dioxide as Reaction Medium. *ACS Catal.* **2016**, *6* (7), 4265–4280. https://doi.org/10.1021/acscatal.6b00848.

(84) Kordikowski, A.; Schenk, A. P.; Van Nielen, R. M.; Peters, C. J. Volume Expansions and Vapor-Liquid Equilibria of Binary Mixtures of a Variety of Polar Solvents and Certain near-Critical Solvents. *J. Supercrit. Fluids* **1995**, *8* (3), 205–216. https://doi.org/10.1016/0896-8446(95)90033-0.

(85) de la Fuente Badilla, J. C.; Peters, C. J.; de Swaan Arons, J. Volume Expansion in Relation to the Gas–Antisolvent Process. *J. Supercrit. Fluids* **2000**, *17* (1), 13–23. https://doi.org/10.1016/S0896-8446(99)00045-5.

(86) Braeuer, A.; Adami, R.; Dowy, S.; Rossmann, M.; Leipertz, A. Observation of Liquid Solution Volume Expansion during Particle Precipitation in the Supercritical CO2 Antisolvent Process. *J. Supercrit. Fluids* **2011**, *56* (2), 121–124. https://doi.org/10.1016/j.supflu.2010.12.015.

(87) van Konynenburg, P. H.; Scott, R. L.; Rowlinson, J. S. Critical Lines and Phase Equilibria in Binary van Der Waals Mixtures. *Philos. Trans. R. Soc. Lond. Ser. Math. Phys. Sci.* **1980**, *298* (1442), 495–540. https://doi.org/10.1098/rsta.1980.0266.

(88) Bolz, A.; Deiters, U. K.; Peters, C. J.; Loos, T. W. de. Nomenclature for Phase Diagrams with Particular Reference to Vapour–Liquid and Liquid–Liquid Equilibria (Technical Report). *Pure Appl. Chem.* **1998**, *70* (11), 2233–2258. https://doi.org/10.1351/pac199870112233.

(89) Deiters, U. K.; Bell, I. H. Calculation of Critical Curves of Fluid Mixtures through Solution of Differential Equations. *Ind. Eng. Chem. Res.* **2020**, *59* (42), 19062–19076. https://doi.org/10.1021/acs.iecr.0c03667.

(90) Bush, D. M. Phase Equilibria of Solid-Supercritical Carbon Dioxide Solutions. Ph.D., Georgia Institute of Technology, United States -- Georgia, 1997.

(91) Sparks, D. L.; Hernandez, R.; Estévez, L. A. Evaluation of Density-Based Models for the Solubility of Solids in Supercritical Carbon Dioxide and Formulation of a New Model. *Chem. Eng. Sci.* **2008**, *63* (17), 4292–4301. https://doi.org/10.1016/j.ces.2008.05.031.
(92) Subramaniam, B.; Rajewski, R. A.; Bochniak, D. J. Process and Apparatus for Size Selective Separation of Micro- and Nano-Particles. US6113795A, September 5, 2000.
(93) Snavely, W. K.; Subramaniam, B.; Rajewski, R. A.; Defelippis, M. R. Micronization of Insulin from Halogenated Alcohol Solution Using Supercritical Carbon Dioxide as an Antisolvent. *J. Pharm. Sci.* **2002**, *91* (9), 2026–2039. https://doi.org/10.1002/jps.10193.
(94) Reverchon, E.; Torino, E.; Dowy, S.; Braeuer, A.; Leipertz, A. Interactions of Phase Equilibria, Jet Fluid Dynamics and Mass Transfer during Supercritical Antisolvent Micronization. *Chem. Eng. J.* **2010**, *156* (2), 446–458. https://doi.org/10.1016/j.cej.2009.10.052.
(95) Raman, S. K.; Kim, H. D. Solutions of Supercritical CO2 Flow through a Convergent-Divergent Nozzle with Real Gas Effects. *Int. J. Heat Mass Transf.* **2018**, *116*, 127–135. https://doi.org/10.1016/j.ijheatmasstransfer.2017.09.019.
(96) Kumar, R.; Mahalingam, H.; Tiwari, K. K. Selection of Solvent in Supercritical Antisolvent Process. *APCBEE Procedia* **2014**, *9*, 181–186. https://doi.org/10.1016/j.apcbee.2014.01.032.
(97) Fouad Ramadan Fouad Zahranra. Microparticles Precipitation Using Supercritical CO2 as an Antisolvent: Role of Thermal Effects and Phase Equilibria, Universidad Complutense de Madrid, 2013.
(98) Villaverde, J. J.; Ligero, P.; de Vega, A. Miscanthus x Giganteus as a Source Of Biobased Products Through Organosolv Fractionation: A Mini Review. *Open Agric. J.* **2010**, *4* (1). https://doi.org/10.2174/1874331501004010102.
(99) Binder, T.; Erpelding, M.; Schmid, J.; Chin, A.; Sammons, R.; Rockafellow, E. *Conversion of Lignocellulosic Biomass to Ethanol and Butyl Acrylate*; Final Technical Report; Archer Daniels Midland Company, Decatur, IL (United States), 2015. https://doi.org/10.2172/1253922.
(100) Taber, D. F.; Patel, S.; Hambleton, T. M.; Winkel, E. E. Vanillin Synthesis from 4-Hydroxybenzaldehyde. *J. Chem. Educ.* **2007**, *84* (7), 1158. https://doi.org/10.1021/ed084p1158.
(101) Handa, S. S.; Khanuja, S.; Longo, G.; Rakesh, D. D. Extraction Technologies for Medicinal and Aromatic Plants. *Int. Cent. Sci. High Technol.* **2008**, 21–25.
(102) Sima, S.; Feroiu, V.; Geană, D. New High Pressure Vapor–Liquid Equilibrium Data and Density Predictions for Carbon Dioxide+ethyl Acetate System. *Fluid Phase Equilibria* **2012**, *325*, 45–52. https://doi.org/10.1016/j.fluid.2012.03.028.
(103) Yun, S. L. J.; Dillow, A. K.; Eckert, C. A. Density Measurements of Binary Supercritical Fluid Ethane/Cosolvent Mixtures. *J. Chem. Eng. Data* **1996**, *41* (4), 791–793. https://doi.org/10.1021/je960032v.
(104) Saitow, K.; Ochiai, H.; Kato, T.; Nishikawa, K. Correlation Time of Density Fluctuation for Supercritical Ethylene Studied by Dynamic Light Scattering. *J. Chem. Phys.* **2002**, *116* (12), 4985–4992. https://doi.org/10.1063/1.1452112.
(105) Byun, H.-S.; Choi, M.-Y.; Lim, J.-S. High-Pressure Phase Behavior and Modeling of Binary Mixtures for Alkyl Acetate in Supercritical Carbon Dioxide. *J. Supercrit. Fluids* **2006**, *37* (3), 323–332. https://doi.org/10.1016/j.supflu.2005.10.007.

(106) Tian, Y.-L.; Zhu, H.-G.; Xue, Y.; Liu, Z.-H.; Yin, L. Vapor−Liquid Equilibria of the Carbon Dioxide + Ethyl Propanoate and Carbon Dioxide + Ethyl Acetate Systems at Pressure from 2.96 MPa to 11.79 MPa and Temperature from 313 K to 393 K. *J. Chem. Eng. Data* **2004**, *49* (6), 1554–1559. https://doi.org/10.1021/je034224j.

(107) Diepen, G. A. M.; Scheffer, F. E. C. The Solubility of Naphthalene in Supercritical Ethylene. *J. Am. Chem. Soc.* **1948**, *70* (12), 4085–4089. https://doi.org/10.1021/ja01192a035.

(108) Camy, S.; Condoret, J.-S. Modelling and Experimental Study of Separators for Co-Solvent Recovery in a Supercritical Extraction Process. *J. Supercrit. Fluids* **2006**, *38* (1), 51–61. https://doi.org/10.1016/j.supflu.2005.03.005.

(109) Peng, D.-Y.; Robinson, D. B. A New Two-Constant Equation of State. *Ind. Eng. Chem. Fundam.* **1976**, *15* (1), 59–64. https://doi.org/10.1021/i160057a011.

(110) Chattopadhyay, P.; Gupta, R. B. Supercritical CO2 Based Production of Magnetically Responsive Micro- and Nanoparticles for Drug Targeting. *Ind. Eng. Chem. Res.* **2002**, *41* (24), 6049–6058. https://doi.org/10.1021/ie020205b.

(111) Liu, S.; Das, L.; Blauch, D. N.; Veronee, C.; Dou, C.; Gladden, J.; Sun, N.; Socha, A. M. Statistical Design of Experiments for Production and Purification of Vanillin and Aminophenols from Commercial Lignin. *Green Chem.* **2020**, *22* (12), 3917–3926. https://doi.org/10.1039/D0GC01234C.

Appendix A: Error

In this work error took two forms, error in repeated measurements, and error in single measurements or calculations. Error in repeated measurements can be calculated by determining the mean of the sample population and the standard deviation of the same population. In this case the reported value is $\bar{x} \pm \sigma$ for the population calculated using Eq. A1 & A2.

$$\bar{x} = \frac{1}{n}\left(\sum x_i\right) \qquad (Eq\ A1)$$

$$\sigma = \sqrt{\frac{\sum(x_i - \bar{x})^2}{N}} \qquad (Eq\ A2)$$

For calculated values e.g., density, recovery, and concentration, propagated uncertainty is used which combines all sources of error related to the calculated value. Each measured value used to calculate the property has its own uncertainty whether it is systematic or random. For a calculated density, both mass and volume are measured, and their respective uncertainties recorded, usually related to the calibration of the balance or volumetric flask. These values, for example would be mass, $m = x \pm u_x$, volume, $v = y \pm u_y$, and density, $\rho = x/y$. Propagating error in calculating density using Eq A3 gives Eq. A4.

$$U_t = \sqrt{\left(\frac{\partial}{\partial x} \cdot u_x\right)^2 + \left(\frac{\partial}{\partial y} \cdot u_y\right)^2 + \left(\frac{\partial}{\partial z} \cdot u_z\right)^2 + \cdots} \qquad (Eq\ A3)$$

$$U_\rho = \sqrt{\left(\frac{\partial \rho}{\partial x} \cdot u_x\right)^2 + \left(\frac{\partial \rho}{\partial y} \cdot u_y\right)^2} = \sqrt{\left(\frac{u_x}{x}\right)^2 + \left(\frac{u_y}{y}\right)^2} \qquad (Eq\ A4)$$

Appendix B: GC Calibration

B.1 Varian CP-3800

The Varian GC was used to analyze chromatography fractions. The fractions were prepared by diluting with MeOH before analysis to decrease the potential to overload the FID. The GC was calibrated using the optimized method described in section 2.3.4 and calibrated over the range of 5-1000 mg/L for both vanillin and *p*HB in AcOH/Toluene/MeOH. This range was chosen based on the observed minimum and maximum solute peak areas. The calibration was separated into low and high ranges due to inflections at high concentrations.

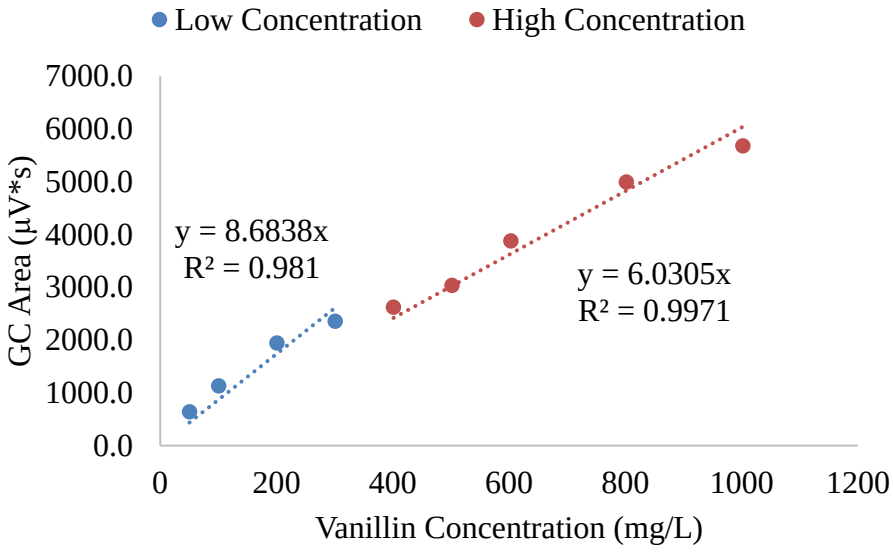

Figure B1: Calibration lines of vanillin at low and high concentrations using the Varian GC. Calibration range of 10-300 and 400-1000 mg/L in AcOH/Toluene/MeOH.

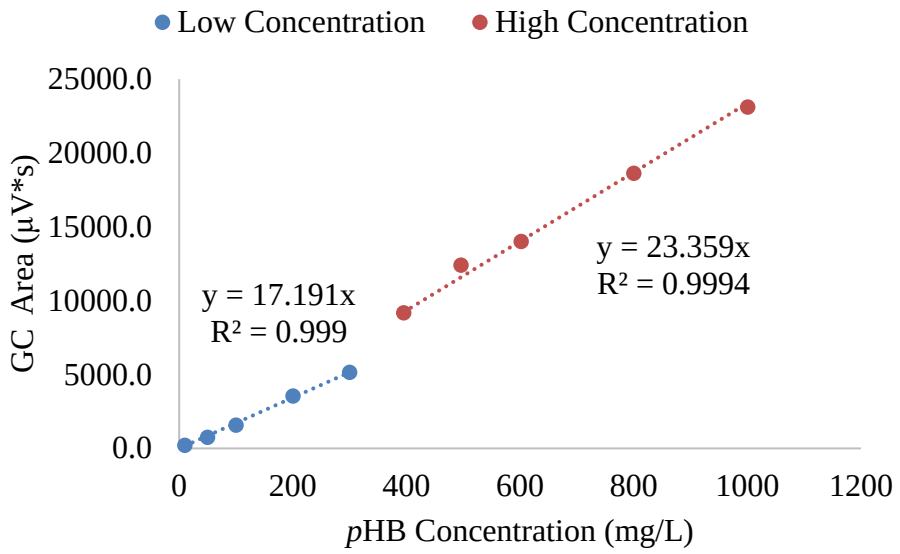

Figure B2: Calibration lines of *p*HB at low and high concentrations using the Varian GC. Calibration range of 5-300 and 400-1000 mg/L in AcOH/Toluene/MeOH.

B.2 Agilent 7890A

The Agilent GC was primarily used to quantify the precipitates from SAS experiments and to verify the calibrations of the Varian GC. In the future this GC will be used to quantify unknowns present in the real lignin mixture chromatography experiments. The calibration range

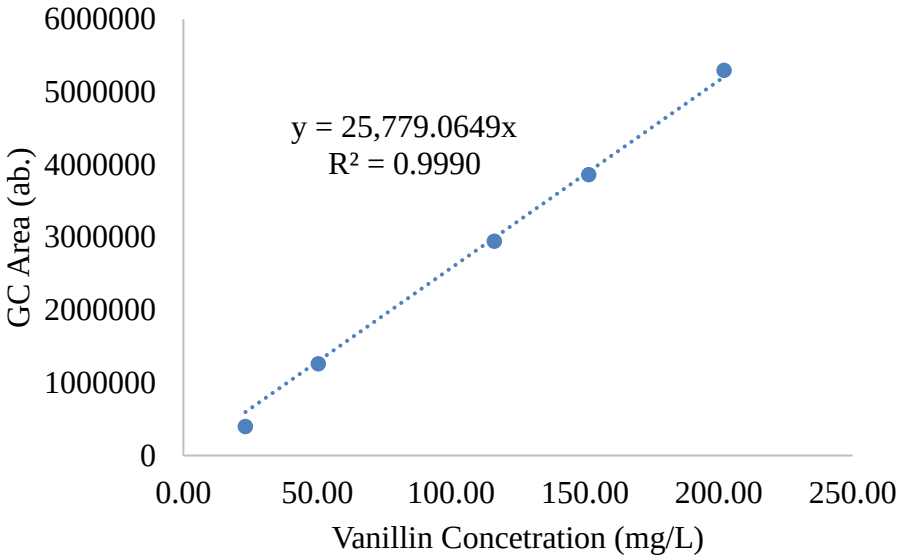

Figure B3: Agilent GC calibration line for Vanillin from 10-200 mg/L in EtOAc.

was 10-200 mg/L for vanillin and *p*HB in EtOAc. A large range is not required because the sample concentration is easier to control.

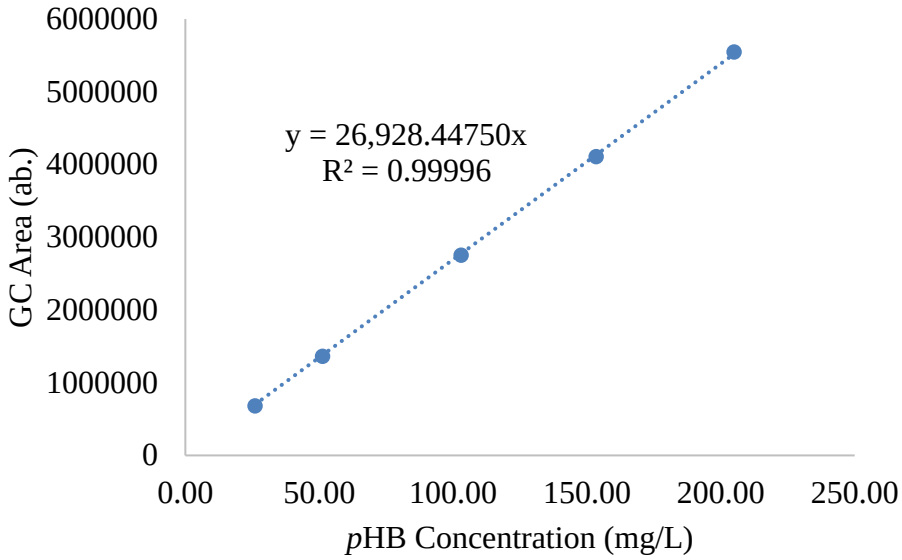

Figure B4: Agilent GC calibration line for *p*HB from 25-200 mg/L in EtOAc.

Appendix C: Run Data

C.1 Chromatography

Example data collected from flash chromatography of vanillin and *p*HB using 15% to 45 v/v % AcOH in toluene.

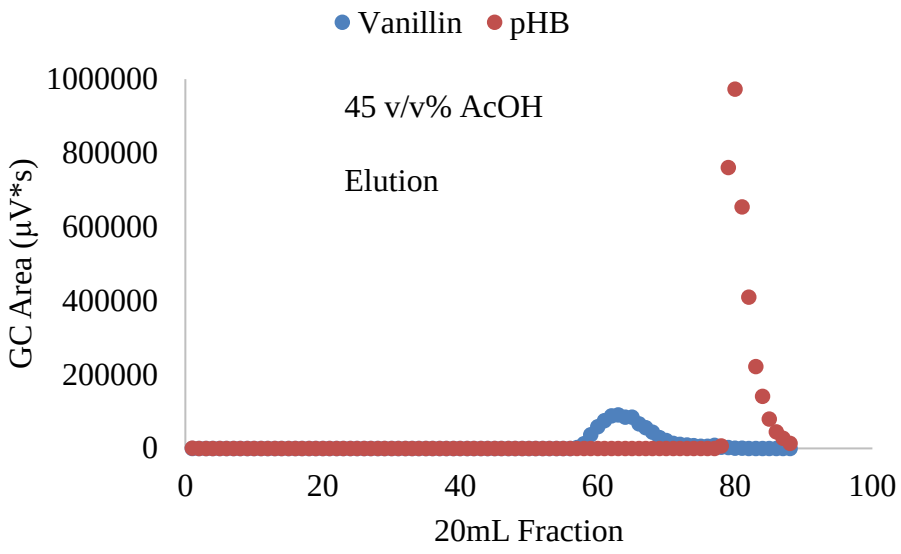

Figure C1: Varian GC area of vanillin and *p*HB in each fraction collected during chromatography.

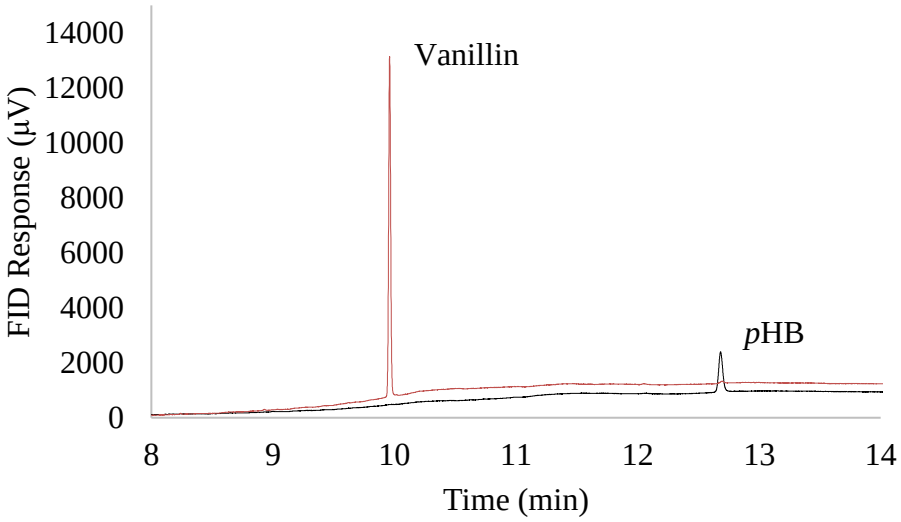

Figure C2: Example FID response of vanillin and *p*HB from the Varian GC. Vanillin has a retention time of 9.96 min and *p*HB is 12.76 min.

C.2 SAS Process

SAS precipitation requires precise control of the pressure regulation valve to maintain constant pressure. Figure C3 is an example of the steps during a SAS precipitation and how those affect pressure and temperature.

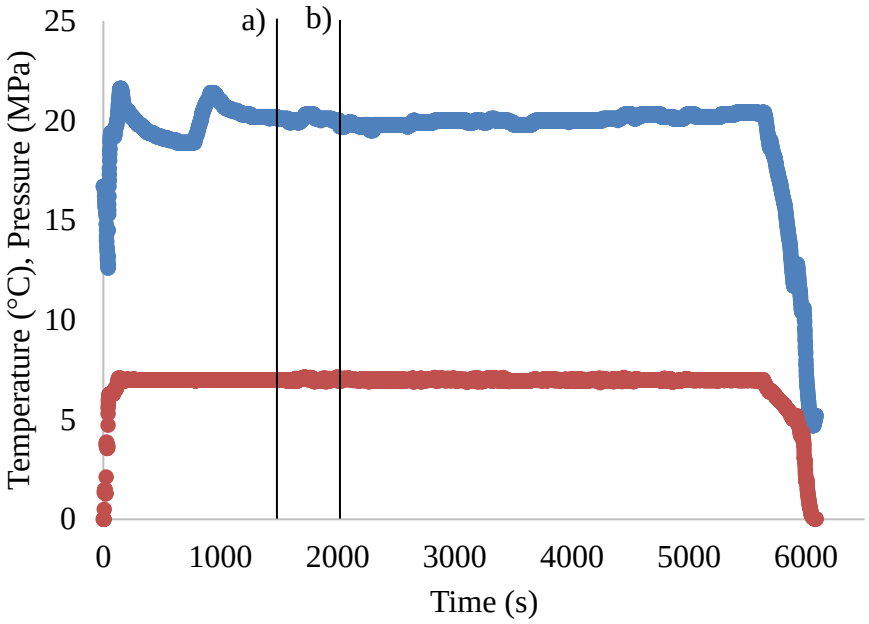

Figure C3: Pressure (blue) and Temperature (red) during an SAS precipitation. Before a), the vessel temperature and pressure are equilibrated. a) represents when the solution is sprayed into the vessel and allowed to equilibrate. b) is the beginning of the SCF wash to remove the solvent. The vessel is then slowly depressurized.

Appendix D: Scanning Electron Microscopy (SEM)

Microscopy was preformed using a Hitachi SU8230 Field Emission SEM. The settings were 10kV accelerating voltage and 9 µA emission current. Crystalline samples were prepared by sputtering 10nm of gold to coat before being imaged. The images show significant morphological and particle size change in vanillin and minor morphologic and particle size reduction in *p*HB.

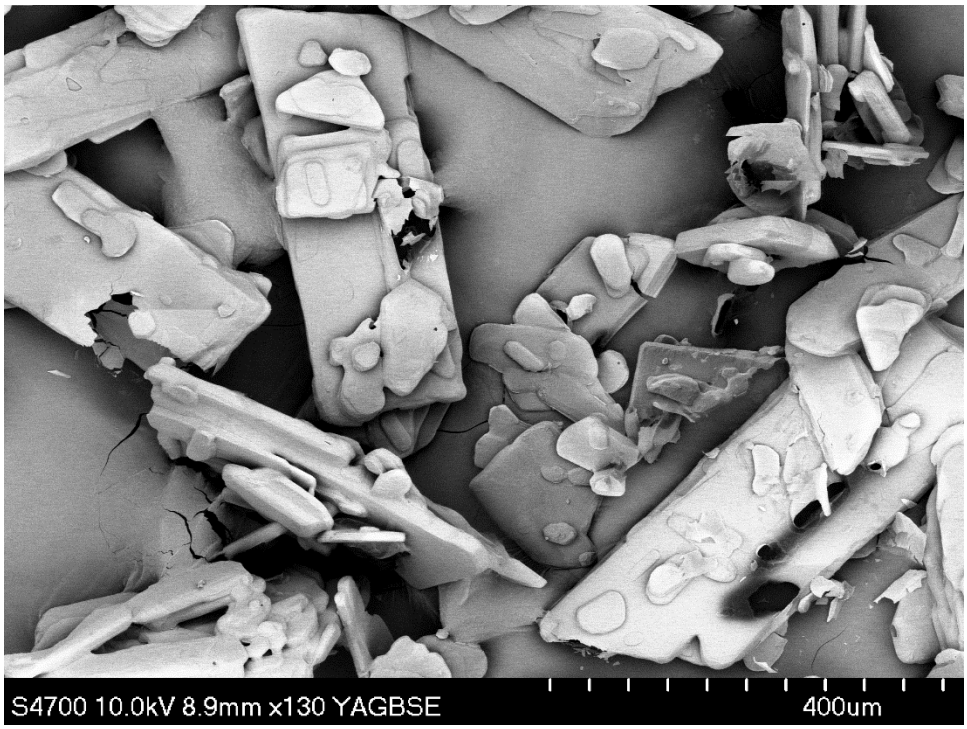

Figure D1: SEM image of gold coated vanillin standard. Average particle size is 105µm.

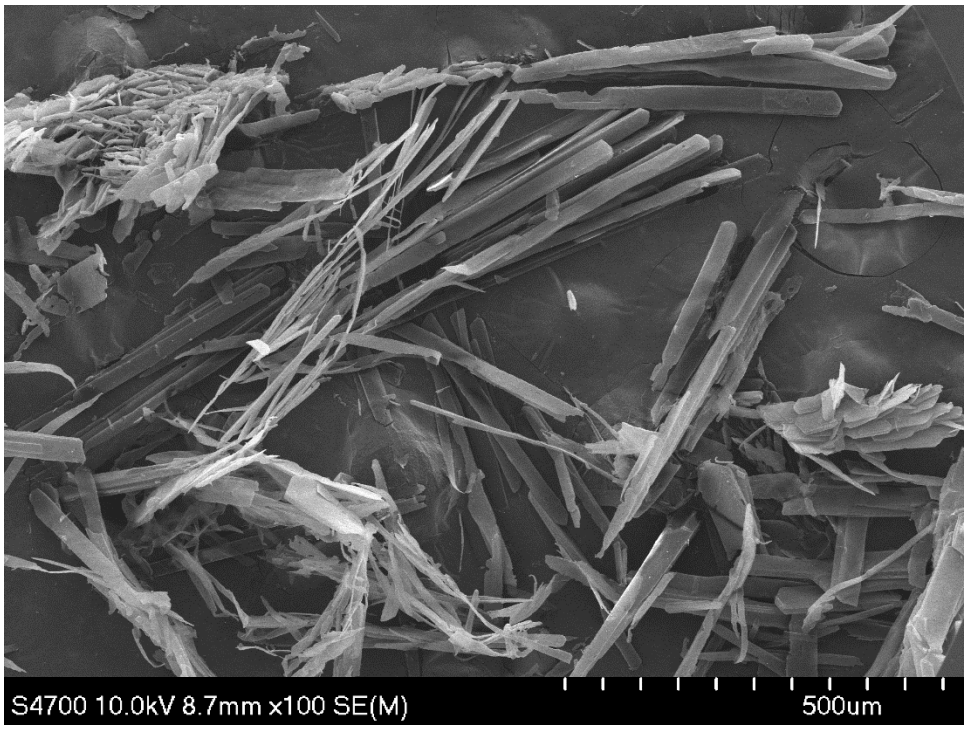

Figure D2: SEM image of gold coated SAS precipitated vanillin. The particles change significantly to thin needles. Average particle size is 30μm.

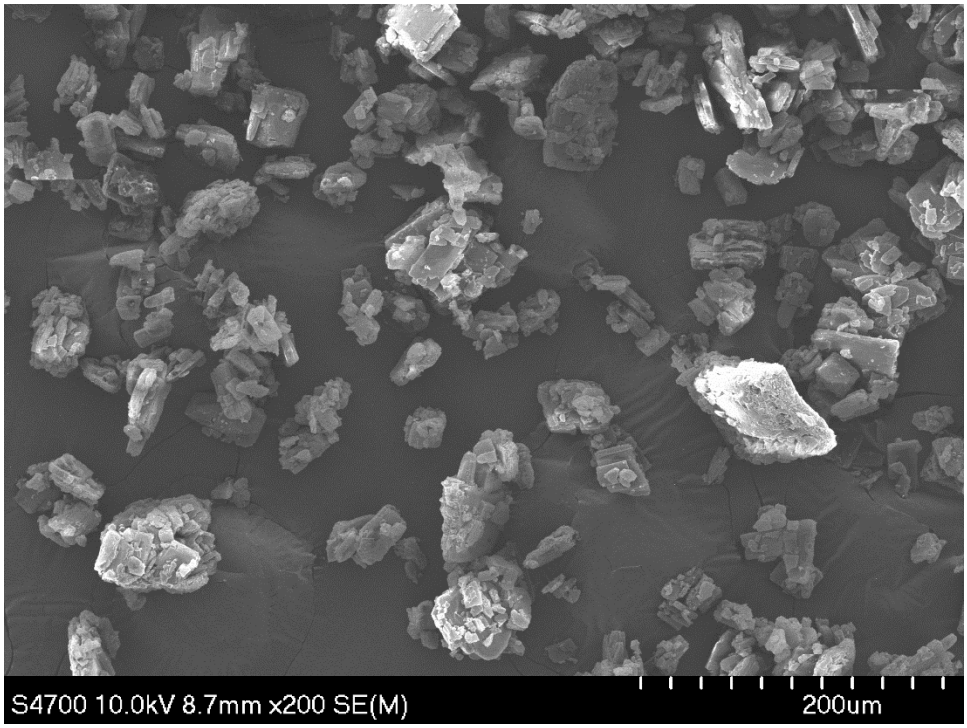

Figure D3: SEM image of gold coated *p*HB standard. Average particle size is 19μm.

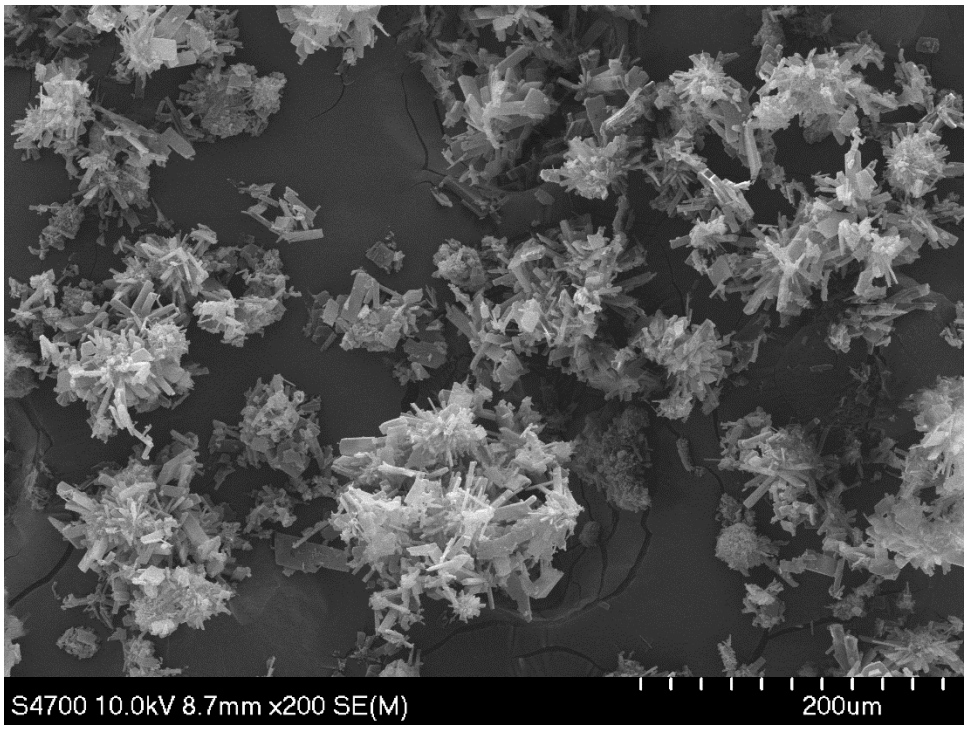

Figure D4: SEM image of gold coated SAS precipitated *p*HB. The particles moderately change to spiked surfaces. Average particle size is 11μm.